THE DEVELOPMENT OF A SMALL ANIMAL MODEL FOR ASSESSING THE 3D IMPLICATIONS OF LOADING ON BONE MICROARCHITECTURE

A Thesis Submitted to the College of

Graduate Studies and Research

In Partial Fulfillment of the Requirements

For the Degree of Masters of Science

In the Department of Anatomy and Cell Biology

University of Saskatchewan

Saskatoon

By

HAYLEY M. BRITZ

In presenting this thesis in partial fulfilment of the requirements for a Postgraduate degree from the University of Saskatchewan, I agree that the Libraries of this University may make it freely available for inspection. I further agree that permission for copying of this thesis in any manner, in whole or in part, for scholarly purposes may be granted by the professor or professors who supervised my thesis work or, in their absence, by the Head of the Department or the Dean of the College in which my thesis work was done. It is understood that any copying or publication or use of this thesis or parts thereof for financial gain shall not be allowed without my written permission. It is also understood that due recognition shall be given to me and to the University of Saskatchewan in any scholarly use which may be made of any material in my thesis.

Requests for permission to copy or to make other use of material in this thesis in whole or part should be addressed to:

Head of the Department of Anatomy and Cell Biology

University of Saskatchewan

Saskatoon, Saskatchewan S7N 5E5

ABSTRACT

It is well established that bone is capable of adapting to changes in its environment; however, little is known regarding how environmental stimuli, specifically loading, are associated with the internal 3D microarchitecture of cortical bone. The aim of this thesis was to develop a small animal model that can be used to experimentally test hypotheses regarding bone adaptation. High resolution micro-CT was validated and employed as a novel method for the visualization and quantification of rat cortical bone microarchitecture in 3D. The use of this imaging method allowed for the measurement of primary vascular canal orientation in 3D, which had never been achieved before. Using this measure along with an immobilization model for unloading allowed me to test how loading is associated with the orientation of these vascular canals. Normally ambulating rat bones (from 10 female rats) had a canal structure that was 9.9° more longitudinal than their immobilized counterparts. This finding that loading has an effect on primary canal orientation brought to light the need to induce remodeling and therefore, secondary vascular canals, in the rat to increase its novelty as a model for looking at bone adaptation. Remodeling was induced by increasing the calcium demands of female rats, either through a calcium restricted diet (n=2) or pregnancy and lactation coupled with a calcium restricted diet (n=2). Mean cortical thickness for the calcium restricted rats and the pregnant and lactating rats that were on a calcium restricted diet were 622 μm and 419 μm, respectively. The mean BMU count for calcium restricted rats seemed to be higher than that of the pregnant and lactating rats; however, the calcium restricted rats seemed to have a lower BMU density. Once this full-scale study is executed the rat will provide a more representative model for studying human bone adaptation.

ACKNOWLDEGEMENTS

I am grateful for the contributions of numerous individuals and institutions that have made this thesis possible. I would like to start off by expressing my greatest thanks to my supervisor, Dr. David Cooper for providing me with the outline of a great project and the direction to complete it when needed. Dave, not only did you bring me to the dark side by deeming me worthy of being your first student at the University of Saskatchewan but you have also instilled in me your enthusiasm for research. I would also like to thank the additional members of my advisory committee, Drs. Saija Kontulainen and Valerie Verge for their insight and assistance over the years.

This thesis would not have been possible had it not been for the generosity and collaborative efforts of Drs. Jarkko Jokihaara, Olli V. Leppänen, Teppo L.N. Järvinen for providing me with the specimens employed in Chapters 2 and 3. Not to mention their feedback regarding the manuscripts that make up these two chapters.

I would like to thank the students and staff of the Department of Anatomy and Cell Biology for their friendship, support and pranking opportunities over the years. In particular, I would like to thank my lab mates Yasmin Carter, Cheryl Hennig, Brian Bewer and Treena Swanston for the laughs and putting up with me on a day-to-day basis. Yasmin Carter deserves further acknowledgement for proofing all of my work, but more importantly, for our daily, caffeine enriched, problem solving sessions.

Financial resources for this research have come from a number of sources and I would like to acknowledge the Natural Sciences and Engineering Research Council of Canada and the University of Saskatchewan for their vital support. A special thanks goes

to Dr. William Kulyk for all of the reference letters he has written for me over the years which have allowed me to secure funding not only for my Masters but my PhD work as well.

My friends deserve a special thanks, for encouraging my competitiveness, assuring me there is life outside the lab and protecting my eyes during the many hours of data analysis while in the lab. Not to mention the opportunity they provide for practicing my networking skills over a pint or two. Nicole Longmuir deserves a special mention for not only being my friend but my roommate for the past six years; I know it cannot be easy living with a mad scientist.

Last, but certainly not least, I would like to acknowledge the support of my family. Without your continual support and understanding this thesis would not have been possible. Thank you mom and dad for the continual support over the years, but most importantly for always encouraging my curiosity and dealing with the numerous 'why' questions. Boys, thanks for being constant reminders of where I come from. Also, thank you for numerous family nights where I occasionally allow you to win.

To my grandmas, a constant source of love, inspiration and cookies.

TABLE OF CONTENTS

LIST OF TABLES

LIST OF FIGURES

LIST OF ABBREVIATIONS

2D	= two dimensional
3D	= three dimensional
BMU	= basic multicellular unit
CT	= computed tomography
Gy	= gray
kV	= kilovolt
mGy	= milligray
Micro-CT	= microcomputed tomography
mm	= millimeter
NO	= nitric oxide
OVX	= ovariectomized
ROI	= region of interest
SR	= synchrotron radiation
vs	= versus
°C	= degrees Celsius
µA	= microampere
µm	= micrometer

CHAPTER 1:

INTRODUCTION

1.1 Introduction

Bone is a metabolically active tissue capable of adapting its structure to various stimuli and repairing structural damage. About 35% of a bone's dry weight is comprised of organic materials, most of which are collagen fibers; the other 65% is largely hydroxyapatite, $Ca_{10}(PO_4)_6(OH)_2$, which is a calcium-phosphate mineral (Pearson and Lieberman, 2004). There are two different bone types which are made up of the same cells and matrix elements: 1) cortical bone, which is very dense and is found in the diaphysis and encloses the medullary cavity and 2) trabecular bone, which refers to the lattice work of thin struts and plates, which are known as trabeculae, in the epiphyses (ends of the bone) (Baron, 2003).

Cortical bone has a highly dynamic microstructure that undergoes continuous change throughout life (Jowsey, 1966). Bone modeling and remodeling are the processes whereby bone is formed and reformed, respectively. Modeling is prevalent during bone growth and is responsible for altering the size, shape and position of tissue in space. Bone formed by modeling is referred to as primary bone and incorporates primary vascular canals that develop into primary osteons (Cooper et al., 2004). Primary bone is an immature form of bone which is abundant in osteocytes and has irregular bundles of collagen (Gartner and Hiatt, 1997). This can be seen in Figure 1.1. Remodeling removes and replaces small packets of primary bone through the initiation of Basic Multicellular Units (BMUs). A BMU contains two main cell types: 1) osteoclasts which resorb bone,

forming what is known as a resorption space (Robling et al., 2006) and 2) osteoblasts that fill in the resorption space with osteoid which mineralizes to form new bone (Robling et al., 2006). The new packet of bone (secondary bone) and its subsequent canal are referred to as a secondary osteon (secondary vascular canal). This secondary bone is considered mature bone, which is composed of parallel or concentric lamella with osteocytes dispersed at regular intervals (Gartner and Hiatt, 1997) (Figure 1.1). The process of remodeling plays an integral part in bone adaptation. Since the 19th century it has been thought that bone's structure is dictated by the loading to which the bone is subjected (Wolff, 1892). The idea that loading dictates bone structure has since been hypothesized to include cortical bone microstructure through the process of bone remodeling. This is evident in studies focusing on the orientation of vascular canals (within primary and secondary bone) in human cortical bone (Hert et al., 1994, Petrtyl et al., 1996).

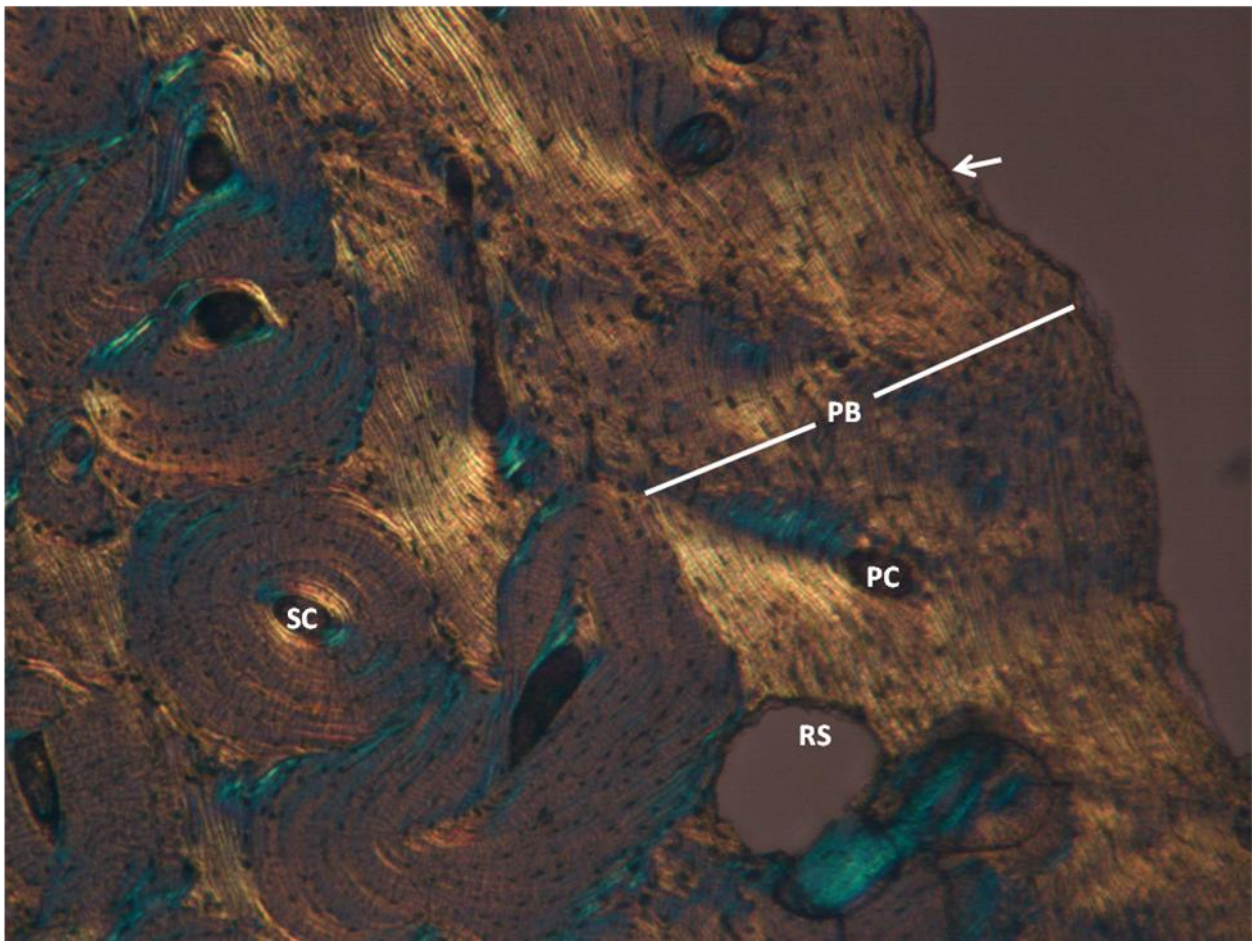

Figure 1.1 – A human femoral ground section viewed under polarized light where the arrow indicates the periosteal (outside) surface, PB is primary bone, PC is primary canal, RS is resorption space and SC is secondary canal. Note: A ground section view of rat bone can be seen in Figure 2.2 on page 17.

Bone is able to sense and respond to loading through a process known as mechanotransduction, the phenomena whereby cells sense mechanical stimuli and translate them into a signal that can potentially elicit some response within the cell or another cell (Pearson and Lieberman, 2004). The cells responsible for sensing mechanical stimuli are osteocytes, which are believed to act as strain receptors and transducers (Marotti, 1996). Where strain refers to a deformation in terms of relative displacement due to stresses generated by a force, such as those produced by loading. There are several hypotheses as to how osteocytes sense strains. Osteocyte canaliculi (long processes that radiate out from the cell body) are filled with fluid, which is displaced when the bone deforms, and the cells are sensitive to pressure changes from these flows, inducing prostaglandin and nitric oxide (NO) production, thereby triggering communication at gap junctions (Bakker et al., 2003, Bakker et al., 2001, Cowin et al., 1995). Strain may also be sensed by the plasma membrane of osteocytes, which contain stretch-activated ion channels that permit calcium flux, which has the potential to initiate other intracellular responses (Davidson et al., 1996, Guggino et al., 1989). Another hypothesis is that small changes in electrical charge are generated by strain-induced fluid flow within the bone matrix (Cowin and Moss, 2001). Dodd *et. al*. (1999) suggested a new hypothesis when they found that the interstitial fluid flow generated by loading is crucial for generating rapid diffusion of oxygen and nutrients to osteocytes. Therefore, in the absence of loading osteocytes would undergo apoptosis due to the lack of oxygen and nutrients, which has been postulated to initiate bone remodeling (Dodd et al., 1999).

It has been suggested that osteoporosis may be due to a reduction in mechanosensitivity and therefore the ability to initiate mechanotrasduction, which would

result in a decrease in the bone's capacity to respond to loading (Klein-Nulend et al., 2002, Seeman, 2004). These studies indicate that osteoporosis may be caused by a defect in the bone's adaptation mechanism (i.e. mechanotransduction). Therefore, model systems that improve our understanding of remodeling may also ultimately improve our understanding of osteoporosis. There are currently two well-established small animal models for studying osteoporosis: the rat ovariectomy (OVX) and the immobilization (IM) induced bone loss models (Jee and Yao, 2001). One of the major shortcomings of using rats is that they have very low levels of intracortical remodeling which results in few secondary osteons. There are two commonly used non-pharmacological ways in which to induce remodeling within the rat 1) introduction of an exercise program (increased loading) and 2) pregnancy and lactation (increased calcium demands). Another limitation of rat models is that their vascular canals are substantially smaller than human cortical bone (Jowsey, 1966). This size differential is problematic in terms of imaging. Vascular canals within human cortical bone can be imaged using desktop micro-computed tomography (micro-CT) (Cooper et al., 2003); whereas, before this thesis work, rat vascular canals were not visualized using this technology (Chapter 2). In order to visualize cortical porosity within a rat, synchrotron radiation micro-computed tomography (SR micro-CT) was needed (Matsumoto et al., 2006, Matsumoto et al., 2007). SR micro-CT uses monochromatic X-rays for CT and the potential advantages of these X-rays have been known since CT was invented (Hounsfield, 1973). In 1983, Grodzins pointed out the suitability of SR for CT (Grodzins, 1983, Zeman and Siddons, 1990). SR micro-CT is able to visualize cortical porosity within a rat due to the monochromaticity of the X-rays, which allow for higher spatial resolutions to be achieved

along with the elimination of beam hardening artefacts, which in turn provide better images for quantification (Dilmanian, 1992).

The primary goal of my thesis is to lay the groundwork for an experimental test of whether loading is a determinant of the 3D orientation of vascular canals. This was done through addressing three objectives 1) deduce whether vascular canals within rat cortical bone can be imaged using a micro-CT 2) assess how immobilization affects primary vascular canals 3) induce remodeling within rat cortical bone. The new 3D perspective on bone adaptation enabled through the combination of high resolution imaging and a small animal model will ultimately shed light on disease processes related to remodeling, such as osteoporosis. The results of these studies will add to the small collection of work looking at the effects loading has on the 3D microarchitecture, more specifically BMUs, of cortical bone using current technology such as desktop micro-CT.

1.2 Organization of the Thesis

The research described within this thesis consists of a series of related studies conducted over the past two years (2009-2011). Chapter 2 compares micro-CT imaging with histology, with the intent of validating micro-CT for the application to rat cortical bone porosity visualization and analysis. The content of this chapter has been previously published in the *Journal of Microscopy* (Britz et al., 2010) and has been reprinted with the permission of John Wiley & Sons, Inc (see appendix B). This study involved a collaboration with Drs. Olli V. Leppänen and Teppo L.N. Järvinen of the University of Tampere, Dr. Jarkko Jokihaara of the University of British Columbia, as well as, Dr. David M.L. Cooper, supervisor. The partnership with Drs. Leppänen, Järvinen and

Jokihaara involved the collection of the specimens utilized in this study. Chapter 2 concludes with a technique for visualizing and quantifying rat cortical porosity using micro-CT that serves as the basis for testing the hypothesis in Chapter 3.

Chapter 3 examines the impact of paralysis (unloading) on cortical vascular canal orientation within the rat tibia using the micro-CT imaging technique developed in Chapter 2. This is achieved through the analysis of Sprague-Dawley rat tibiae that had been paralyzed at 3 weeks of age by sciatic neurectomy (n=10) for 27 weeks (left hind limb), the tibiae from the same rat's SHAM operated right hind limb (n=10; internal control) and these rat's age and sex matched external control tibiae (n=10) from the left hind limb of normally ambulating rats. This sample was derived from a previous study conducted by Drs. Leppänen, Järvinen and Jokihaara and the external controls were used in the study performed in Chapter 2 of this thesis. The hypothesis that vascular canals align themselves along the dominant loading direction was tested in this chapter.

Chapter 4 describes a pilot study, which explores different methods for inducing cortical bone remodeling in the rat tibia. The hypothesis that calcium restriction alone provides a great enough increase in calcium demand to induce remodeling is characterized. Achieving a better technique for inducing cortical bone remodeling in the rat will provide researchers with an overall better animal model for osteoporosis that can be easily manipulated to test different hypotheses. More specifically, the question "do BMUs align themselves along the dominant loading direction as vascular canals seem to do" was explored.

Chapter 5 concludes this thesis with an overview of the results from the studies conducted in Chapters 2 through 4 and a discussion of future research directions.

1.3 Summary

The information gained from having a technique of induced remodeling in rats with the ability to subsequently subject them to experiments examining the effects of loading and unloading will provide researchers with an easily manipulated experimental model for looking at bone adaptation, which can more readily be used to make comparisons with human bone. This technique will also represent a more unique model of osteoporosis, which can then be employed to look at whether or not the large resorption spaces within the cortex of osteoporotic bone are a result of coalescing remodeling events due to a problem in the bone's mechanism of adaptation. If this turns out to be the case, then there will be evidence that physical activity needs to be more strongly encouraged in the older population in order to protect against this disease.

This rat model for assessing the 3D implications of loading on rat cortical bone microarchitecture can also be applied to other disciplines such as paleontology and physical anthropology. These two fields rely on skeletal material to make inferences about a wide range of subjects including taxonomy, evolutionary relationships, life history and behavior (Pearson and Lieberman, 2004). Knowing how loading affects the microarchitecture of cortical bone, such as the orientation of canals, will allow specialists in these fields to more accurately infer behavioral movements from the fragments of bone they receive.

CHAPTER 2:

3D VISUALIZATION AND QUANTIFICATION OF RAT CORTICAL BONE POROSITY USING A DESKTOP MICRO-CT SYSTEM: A CASE STUDY IN THE TIBIA

2.1 Introduction

The use of micro-CT for the 3D assessment of bone structure *in vitro* was introduced by Feldkamp *et al.* in 1989 (Feldkamp et al., 1989). Since then, this technology has become the gold standard for assessing the 3D architecture of trabecular bone. The primary advantage of micro-CT is its ability to efficiently provide non-destructive quantitative results with little or no preparation of the sample. Previous methods for 3D analysis of bone involved applying theorems of stereology (Parfitt et al., 1983) to large numbers of 2D serial sections. Substantial preparation is involved in obtaining these serial sections, which is time-consuming and ultimately results in the destruction of the specimen.

2.1.1 Application of Micro-CT for Imaging Trabecular Bone

Early anatomists found that trabecular bone microstructure varied due to the mechanical forces normally experienced by the bone; therefore, perceiving it as a material of optimal design (Koch, 1917). Trabecular bone is made up of a series of plates and connecting rods. During aging and disease such as osteoporosis there is a continuous shift from one structural type to the other (Jiang et al., 2000) which is difficult to analyze using the traditional technique for analyzing trabecular bone structure stated above. Numerous papers have been published using micro-CT to quantitatively analyze

trabecular bone (Barbier et al., 1999, Barou et al., 2002a, Barou et al., 2002b, Fajardo et al., 2002, Ito et al., 1998, Kuhn et al., 1990, Muller et al., 1996, Muller et al., 1998, Uchiyama et al., 1997) since it has been found to be a more accurate technique for quantitatively analyzing this tissue. Also, the ability to both capture the trabecular structure and reuse samples for biomechanical tests which are afforded by the use of micro-CT are also paramount to testing bone strength since it has been found to be closely related not only to bone mass but also trabecular bone structure (Kleerekoper et al., 1985, Recker, 1993).

2.1.2 Application of Micro-CT for Imaging Human Cortical Bone

The application of micro-CT to trabecular bone has become commonplace; however, the assessment of the smaller-scale internal structures within compact cortical bone has been more limited. The cortical bone of many vertebrates has a complex and dynamic microstructure that continually remodels throughout life. Remodeling-related change affects bone strength (Carter et al., 1976) and is linked to the functional adaptation of bone as well as disease states (e.g. osteoporosis). As such, analysis of cortical microstructure in 3D holds great potential to shed new light on a number of important areas of bone biology. That said, visualization of the products of remodeling (secondary osteons) in 3D using serial histology has been limited in scope and largely qualitative in nature (Cohen and Harris, 1958, Mohsin et al., 2002, Stout et al., 1999, Tappen, 1977). Attempts to directly detect secondary osteons with desktop micro-CT have not been very successful per se (Cooper et al., 2004); however, the vascular canals, which lie at the centre of each osteon, can be visualized and quantified with this technology (Cooper et al., 2003). The vascular canals of cortical bone make up an

interconnected network, which is altered by remodeling. Three-dimensional analysis of the canal network provides insights into cortical bone structural dynamics at this level (Cooper et al., 2007b). A growing number of studies have employed desktop micro-CT to analyze human cortical bone porosity (Basillais et al., 2007, Borah et al., 2009, Chen et al., 2009, Cooper et al., 2007a, Cooper et al., 2004, Cooper et al., 2003, Feldkamp et al., 1989, Jones et al., 2004, Renders et al., 2007, Wachter et al., 2001); however, to my knowledge, it has never been applied to the cortical microstructure of a small animal, such as the mouse or rat.

2.1.3 Application of SR Micro-CT for Imaging Rat Cortical Bone

To date, the ability to analyze the cortical microstructure of a small animal, such as the mouse or rat, which is challenging due to the smaller scale of the vascular canals, has only been achieved through the use of synchrotron radiation (SR) micro-CT. The use of a synchrotron X-ray source provides advantages beyond desktop micro-CT including higher spatial resolution (Peyrin et al., 2000), greater X-ray flux and the capacity to utilize a monochromatic beam which eliminates beam hardening artefacts and, therefore, provides better images for quantification (Dilmanian, 1992). The application of SR micro-CT to cortical bone porosity has included the analysis of not only human femoral specimens (Bousson et al., 2004) but also rats (Matsumoto et al., 2006, Matsumoto et al., 2007) and mice (Schneider et al., 2009, Schneider et al., 2007).

2.1.4 Study Objectives

Although a synchrotron affords many advantages, access and beam time are limited at such facilities. As such, the capability to achieve a comparable level of imaging in a laboratory setting is highly desirable and could substantially accelerate research in

this relatively unexplored area of bone biology. Thus, the primary goal of this study was to determine if it is possible to visualize and quantify cortical bone porosity in the rat using a commercially available high-resolution desktop micro-CT scanner and to validate the results against conventional histological analysis.

2.2 Materials and Methods

2.2.1 Specimens

The right tibiae from 10 skeletally mature (30-week-old) Sprague-Dawley rats used in the current study were collected from control rats in a previous study (using the femora) which was conducted by one of my collaborators (Teppo Järvinen) at the University of Tampere, Finland. Ethics approval for collection and study was granted by the Ethics Committee for Animal Experiments of the University of Tampere and the Provincial Government of Western Finland Department of Social Affairs and Health, Finland. For the current study, approval was granted by the University of Saskatchewan Biomedical Research Ethics Board (permit #20080050; see appendix A). The rats were housed in cages (16 x 27 x 42 cm), two animals per cage, at 20 °C with a light cycle of 12 hours and had access to food and water *ad libitum*.

2.2.2 Micro-computed Tomography

Micro-CT images will be referred to as *slices* and the ground sections as *sections* in accordance to the convention of Kuhn *et al*. (Kuhn et al., 1990). Subsamples of the tibiae were cut using an Isomet 1000 slow speed saw (Buehler, Lake Bluff, IL, U.S.A.) at the tibia-fibula junction and immediately distal to the tibial crest (Figure 2.1). This segment of bone was then soaked in 3% hydrogen peroxide for 3 days to clear soft tissue

and then allowed to air dry. These samples were scanned using a SkyScan 1172 (Kontich, Belgium) X-ray microtomograph (< 5 µm X-ray source spot size; 8.83 camera pixel size). The samples were rotated through 360 degrees at a rotation step of 0.09 degrees. The X-ray settings were standardized to 100 kV and 100 µA, with an exposure time of 0.2 seconds per frame. Two-frame averaging was used to improve the signal-to-noise ratio. A 1-mm-thick aluminum filter and a beam-hardening correction algorithm were employed to minimize beam-hardening artefacts (SkyScan hardware/software). The scan time for each sample was approximately 3 hours. Each scan produced 1124 contiguous slices with a nominal resolution of 3 µm. To reduce image noise and preserve detail in three dimensions, the image series was passed through a 3D median filter with a 3 x 3 x 3 cubic kernel (SkyScan software). These images were analyzed using CT Analyzer 1.9.1.0 (SkyScan software). A circular region of interest (ROI) with a 1 mm diameter was placed with one edge touching the periosteal surface of the anterior part of the bone (Figure 2.1). This ROI was isolated to facilitate a direct comparison with histological measures (see below) and the anterior crest provided the largest field within the tibia. For the micro-CT datasets, the 2D ROI was extended through 200 slices (0.6 mm) to create a cylindrical volume of interest. The canals were identified using a standardized global threshold and the binarized dataset was then 'despeckled', removing 3D objects that consisted of less than 25 voxels – which I assumed to be noise. Percent porosity (canal volume fraction) and mean canal diameter were measured as described by Cooper *et al*. (Cooper et al., 2003). Canal diameter was measured using a model-independent distance transform based on Euclidean distance (see Jones et al., 2009, Mickel et al., 2008 for reviews) where the diameter at a specific point in the structure is the diameter of the largest sphere

which can fit completely inside the 3D structure, which was first used to extensively measure trabecular thickness in bone (Hildebrand and Ruegsegger, 1997) and has since been used to measure canal diameter in cortical bone (Cooper et al., 2003). SkyScan software (CTAn and CTVol) was employed to make 3D renders of cortical bone porosity using the double-time cubes method.

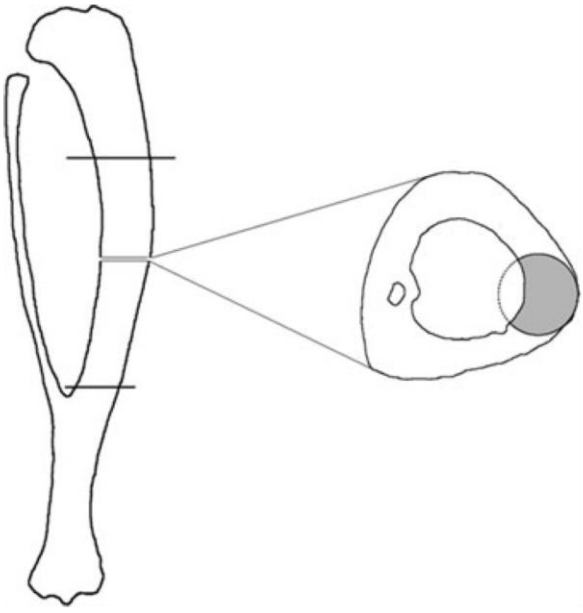

Figure 2.1 – A schematic of the rat tibia and the area scanned along with a cross-section depicting a shaded-in region of interest (ROI).

2.2.3 Ground Section Histology

After scanning, the bone specimens were embedded in EpoThin epoxy resin (Buehler, Lake Bluff, USA) before being placed into an Isomet 1000 slow speed saw (Buehler, Lake Bluff, USA) and five subsequent cuts were made, starting at the proximal end. These cuts were made at 0.25 mm intervals. The third and fifth sections from each bone were ground down between two pieces of 2000 grit sand paper until they were 100 microns thick, using a technique adapted from Frost (Frost, 1958). The 100 µm sections were placed in hydrogen peroxide for a minute before being put in an ultrasonicator to remove the fine grit. The sections were imaged using a SONY DSC-V3 camera on a Leica LEITZ DMR microscope. Images of the anterior portion of the tibiae were taken at 20X magnification (tiled to cover the whole region). These images were analyzed using the ImageJ software platform (v1.40G, NIH; http//rsb.info.hih.gov/ij/). Built-in capabilities of ImageJ and custom written macros were employed. For each image a circular ROI, with a 1 mm diameter, was placed with one side touching the periosteal surface. The size and location of this ROI corresponded to that used in CT Analyzer to assess the micro-CT slices. Within the ROI all canals were manually outlined using an interactive LCD tablet (Cintiq 12WX model, Wacom Co. Ltd., Japan). The following measurements were obtained: percent porosity which represented the percent of the bone area within the ROI that was occupied by canals; canal diameters were measured as the mean of the central ridge after a two-dimensional Euclidean distance transform of the canal outline. The percent porosity and mean canal diameter were averaged across the two sections from each specimen and these values were utilized for quantitative comparisons against the micro-CT datasets. Qualitative comparisons were made against

average projections through 33 micro-CT slices, to approximate an equal thickness of bone in both the slices and sections.

2.2.4 Statistical Methods

All statistical analysis was performed using SPSS 16.0 (SPSS Inc., Chicago, IL, USA). Overall mean values for percent porosity and mean canal diameter were calculated from the individual specimen values (n=10) from both the micro-CT datasets and histological sections. The results from the two methods were compared in accordance with the approach outlined by Altman and Bland (Altman and Bland, 1983). Briefly, this approach involves plotting the difference between two methods against their mean. Bias is defined as the mean difference between the two techniques. In this case, the micro-CT results were subtracted from the histological results. Paired T-tests were performed with significance $\alpha < 0.05$ to compare the two methods and provide information on the significance of the differences.

2.3 Results

Cortical canals were clearly visualized in the micro-CT slices. Histological sections matched up well with the average projections through 33 slices as seen in Figure 2.2. The cutting cones of active basic multicellular units (BMUs) were also occasionally discernable (Figure 2.3). The average percent porosity was found to be 2.6 % ± 1.0 % for the histological sections and 2.8 % ± 1.1 % for the micro-CT slices. The average canal diameter was found to be 11.5 µm ± 1.35 µm in the histological sections and 17.2 µm ± 1.91 µm from the micro-CT slices. Figures 2.4 and 2.5 show Bland-Altman plots for percent porosity and canal diameter, respectively. The bias (± 95% confidence interval)

for percent porosity was -0.2 % (± 2.6 %). Canal diameter had a bias (± 95% confidence interval) of -5.73 μm (± 4.02 μm) as seen in Figure 2.5. Paired T-tests revealed the bias for percent porosity not to be significantly different from zero ($p=0.720$), whereas, it was found to be significantly different when considering canal diameter ($p<0.001$).

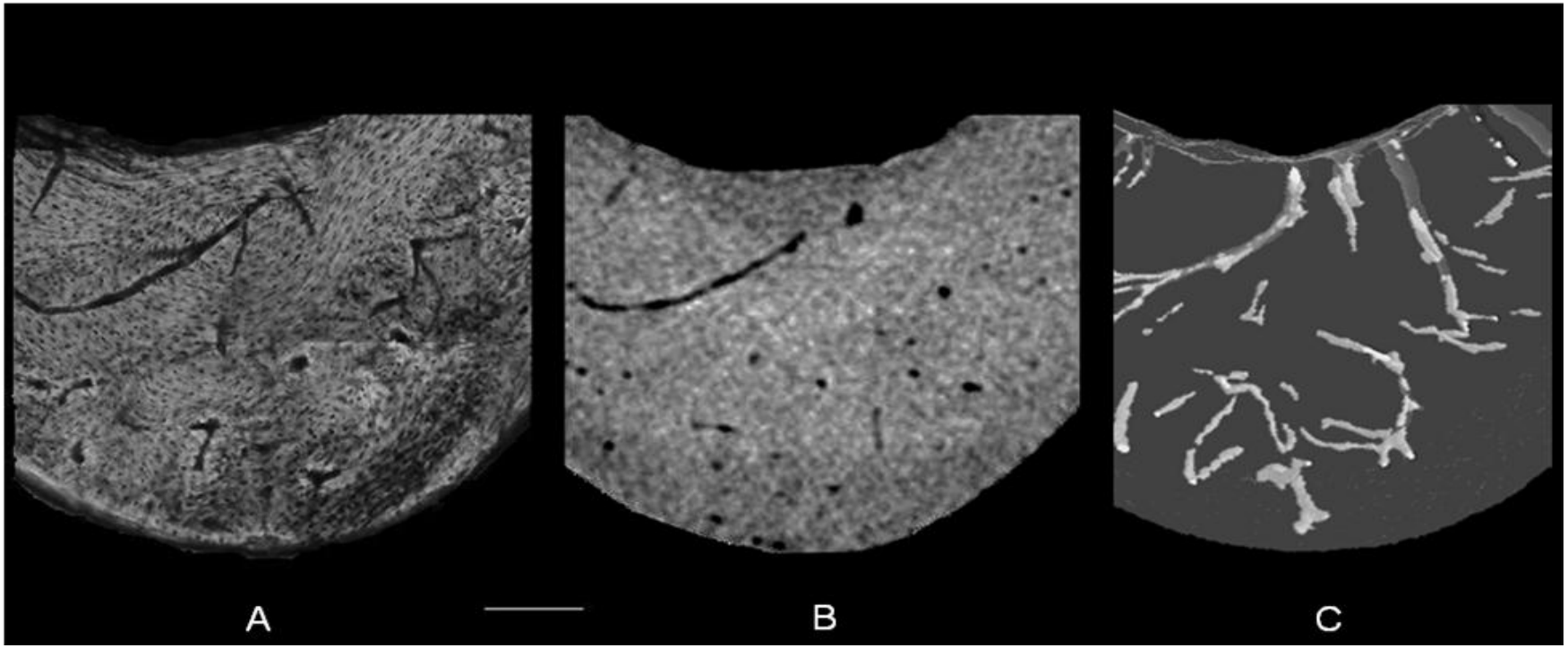

Figure 2.2 – Anterior portion of a tibial cross-section from a 100 µm ground section (A), micro-CT projection through 33 slices (B), 3D render of 33 micro-CT slices (C). Three hundred micro-CT slices are equal in thickness to 100 µm. Bar = 200 µm.

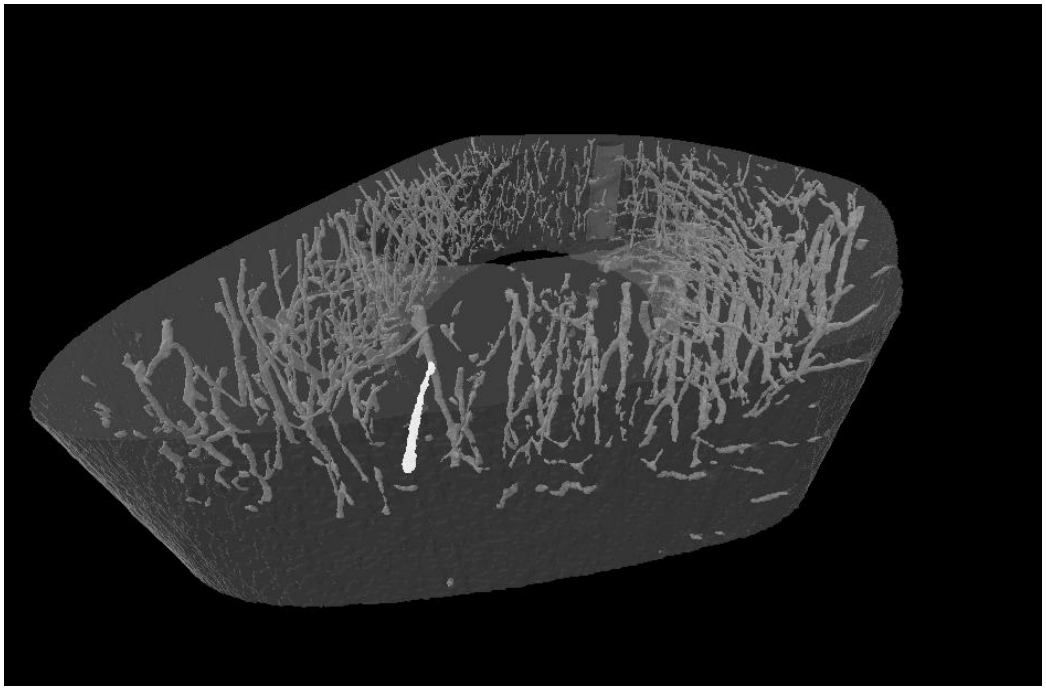

Figure 2.3 – A 3D rendering of the canals in a piece of rat cortical bone with a highlighted basic multicellular unit (BMU).

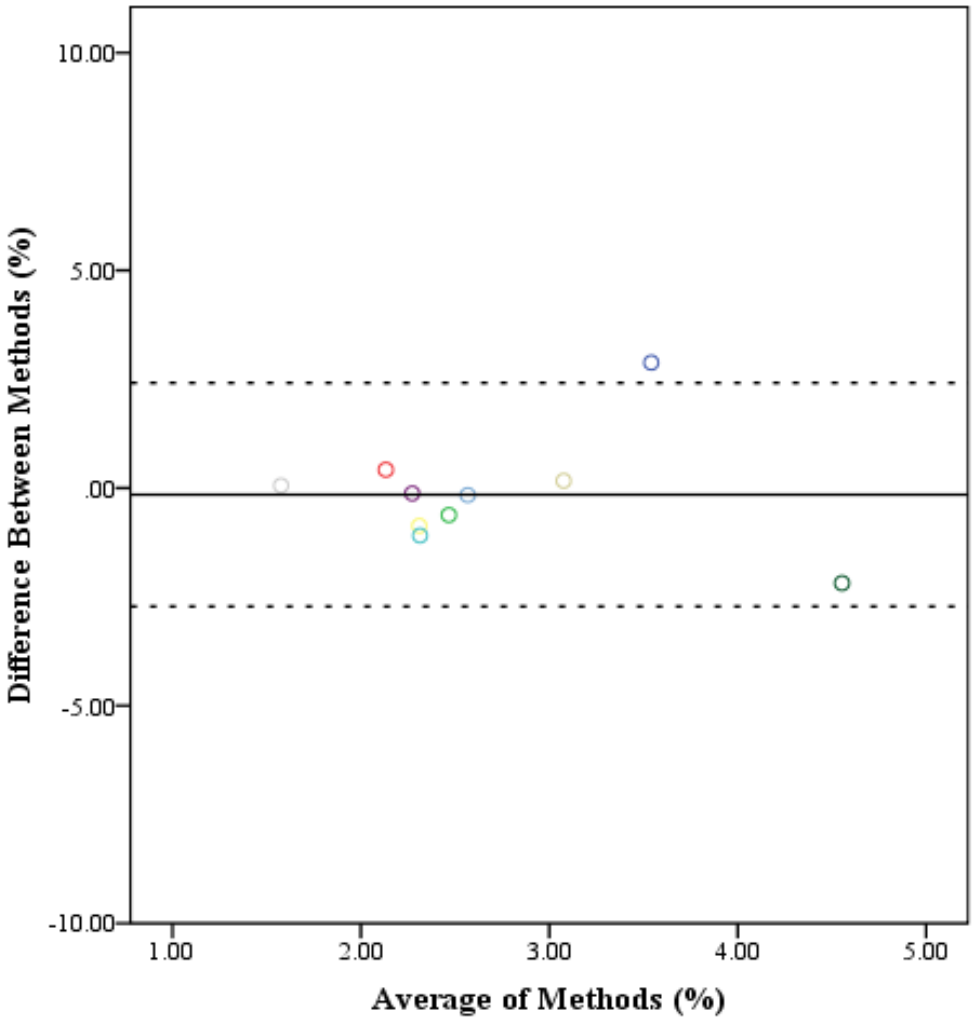

Figure 2.4 – Bland-Altman plot of the differences between micro-CT and histology for measuring cortical porosity (%). The same 10 specimens were used for both micro-CT and histology. Paired T-tests revealed the bias for percent porosity was not significantly different from zero (p=0.720); therefore micro-CT can be used to measure cortical porosity.

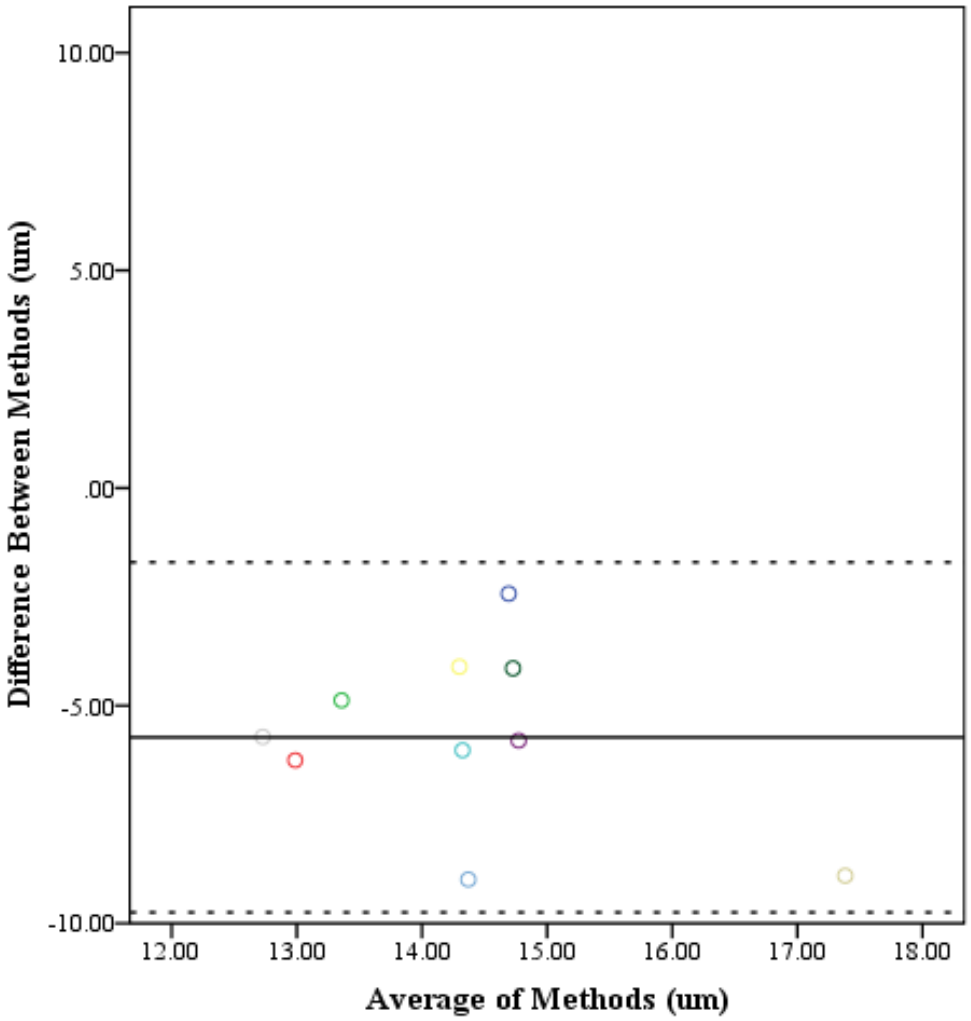

Figure 2.5 – Bland-Altman plot of the differences between micro-CT and histology for measuring canal diameter (µm). The same 10 specimens were used for both micro-CT and histology. Paired T-tests revealed the bias for canal diameter was significantly different from zero ($p<0.001$); therefore, micro-CT overestimates canal diameter by about 5 µm.

2.4 Discussion

There have been numerous micro-CT validation studies for trabecular (Feldkamp et al., 1989, Hildebrand et al., 1999, Kuhn et al., 1990, Muller et al., 1998) and cortical bone (Cooper et al., 2004, Wachter et al., 2001); however, none have looked at the cortical porosity of a small animal model such as the rat. This study is the first of its kind to show that it is possible to visualize the porosity within rat cortical bone using a desktop micro-CT and to validate quantitative results against conventional histology. The matches between the micro-CT slices and corresponding histological sections provided qualitative validation of the approach (Figure 2.2). These matches were often not as precise as those depicted in a previous validation study of human cortical bone (Cooper et al., 2004); however, the cortical canals within human cortical bone are substantially larger than those found in rats and generally longitudinally oriented. The far greater frequency of radial canals in the rats created difficulty in achieving precise matches as slight variations in orientation created far greater changes in apparent morphology. From a quantitative perspective, the percent porosity measures were more comparable to histology than were measures of canal diameter. This supports a previous finding by Muller *et al*. (Muller et al., 1998).

The only previous work to examine rat cortical porosity in 3D is that of Matsumoto and colleagues (Matsumoto et al., 2006, Matsumoto et al., 2007) which employed SR micro-CT (Spring8, Japan). In two published studies, they used a nominal resolution of 5.83 μm to image a portion of the tibia similar to that assessed in the current study. Their studies generated percent porosities of 1.7 % (Matsumoto et al., 2006) and 2.0 % (Matsumoto et al., 2007) for control specimens. These values are slightly lower

than those I obtained (2.8 %). With respect to mean canal diameter, my value from micro-CT was 11.5 µm, this time slightly lower than the values obtained by Matsumoto *et al*. at 13.9 µm (Matsumoto et al., 2007) and 17.5 µm (Matsumoto et al., 2006). These differences can be attributed to a number of variables including differences in strain (Wistar vs. Sprague-Dawley rats), age (14 weeks vs. 30 weeks), sex (male vs. female) nominal scan resolution (5.84 µm vs. 3 µm), imaging system (synchrotron vs. micro-focus source), analytical software, etc. The two most notable factors were differences between the synchrotron and desktop system and the maturation of the specimens. Bernhardt *et al*. (Bernhardt et al., 2004), for example found there to be considerable differences in results depending on the type of scanning system used and cautioned against directly comparing results. Further, the impact of age differences was likely significant as rats undergo rapid growth until 8 weeks and then a stage of slower, steady growth continues (Bennell et al., 2002). Thus, the specimens used in the current study were derived from considerably more mature rats than those used by Matsumoto *et al*. (Matsumoto et al., 2006, Matsumoto et al., 2007).

Although Matsumoto and colleagues conducted qualitative validation by comparing histological images against SR micro-CT image data, they did not conduct a quantitative validation. In the comparison carried out in this study, the results for percent porosity from micro-CT were in very close agreement with those from histology. The bias for percent porosity was found to be -0.2 %, which indicates the micro-CT was slightly overestimating porosity but this difference was not significant. For mean canal diameter, a significant ($p<0.001$) bias of -5.73 µm between the techniques with micro-CT overestimating relative to histology this time. Although some of the discrepancy between

the two techniques is attributable to differences in the specific region analyzed and the nature of the measurements (2D vs. 3D), in general the results are consistent with a pattern whereby the 3 μm nominal resolution (<5 μm X-ray source spot size) was insufficient for detection/segmentation of the smallest of canals. When the size of the target object approaches the spatial resolution of the scan, the averaging effect has an increasing affect on the scan (Cooper et al., 2004); the edges of the object will appear blurred and this can lead to difficulties with segmentation. Further, post-acquisition modifications such as median filtration, although necessary to suppress noise, also blur fine details. The loss of small canals to the partial volume effect could explain why my values for mean canal diameter were inflated although overall percent porosity was concomitantly deflated. Notably, a similar pattern of results was found in a study validating 2D micro-CT and histological measures in human cortical bone. Cortical porosity was not significantly biased between the methods although pore area was (Cooper et al., 2004). This differential stability of results for overall thickness/diameter has been described previously in resolution dependency studies of trabecular (Muller et al., 1996) and cortical bone (Cooper et al., 2007a).

The results of this study also revealed that micro-CT imaging of rat cortical bone faces the same limitations observed in human bone studies. For example, I was unable to differentiate between the types of canals present because fine structural details such as osteonal cementing lines/lamellae were not visible in the micro-CT slices (Cooper et al., 2007a). To achieve such a level of imaging, it may, ultimately, be necessary to utilize SR micro-CT. The improved resolution of such systems has already enabled the visualization and quantification of osteocyte lacunae in the mouse (Schneider et al., 2009, Schneider et

al., 2007). Further, phase contrast techniques have enabled SR micro-CT to non-invasively assess dental microstructures that are similar in scale to bony lamellae (Tafforeau and Smith, 2008). Although SR micro-CT has many advantages, it has a major disadvantage – limited access. Thus, although desktop micro-CT systems cannot rival the capabilities of SR micro-CT, they offer a more accessible alternative for certain levels of imaging.

2.5 Conclusion

Many studies have employed micro-CT to qualitatively and quantitatively analyze cortical porosity within human bone. The aim of this study was to establish desktop micro-CT as a more readily available way to quantify cortical porosity in a small animal such as the rat. This study has demonstrated that cortical porosity imaging in the rat is indeed possible in a laboratory setting with commercially available equipment. This finding will greatly expand access and accelerate research in the area of 3D cortical bone structure.

CHAPTER 3:

THE EFFECTS OF IMMOBILIZATION ON VASCULAR CANAL ORIENTATION IN RAT CORTICAL BONE

3.1 Introduction

Bone is a metabolically active tissue capable of adapting its structure to mechanical stimuli and it is capable of repairing structural damage. Bone adaptation and structural repair occurs in 3D and therefore, cannot be fully characterized using 2D methods. For this reason Chapter 2 introduced the application of micro-CT for 3D visualization and quantification of cortical bone porosity in the rat. The current chapter used the micro-CT technique developed in Chapter 2 to obtain 3D images that can be employed for measuring vascular canal orientation in rat cortical bone. The study described in this chapter tested the effect of immobilization (unloading) on these measures of vascular canal orientation.

3.1.1 Bone Adaptation to Mechanical Loading

It has been over a century since it was first recognized that bone adapts its structure to the mechanical forces exerted upon it. The ability of bone to adapt its structure to its mechanical environment allows it to remain structurally sound and endure the loads it is exposed to without breaking. In 1892, Julius Wolff found that trabeculae within the femoral neck align in the direction of the principal stress (Wolff, 1892). Since this discovery, loading has been shown to affect bone length (Howell, 1917, Steinberg and Trueta, 1981), mass (McDonald et al., 1986, Raab et al., 1991, Turner and Bell, 1986), shape (Rubin, 1984), cross section (Bennell et al., 2002, Uhthoff and Jaworski,

1978) and strength (Järvinen et al., 2003b, Leppänen et al., 2008). Most recently, the focus of studies involving mechanical loading and bone adaptation have been centered on how secondary osteons are affected. Using either *in silico* (Baca et al., 2007, Burger et al., 2003, Smit and Burger, 2000, Smit et al., 2002, van Oers et al., 2008b), histologic (Lanyon and Bourn, 1979) or ink-based (Hert et al., 1994, Pazzaglia et al., 2008, Petrtyl et al., 1996) techniques it has been found that osteons align themselves parallel to the loading direction. In regards to the effect of loading on osteon geometry, Young *et al.* found that an increase in strain resulted in a decrease in osteon size in monkeys (Young et al., 1986). A similar finding was later reported in humans, when Britz *et al.* showed osteon diameter to be lower in heavier people (Britz et al., 2009).

While most research in this area has focused on secondary osteons, the orientation of primary cortical structures has also been linked to loading. In 2002, de Margerie found that bones subjected to different loading patterns (strain mode) had different degrees of laminarity, where laminarity is a measure of vascular orientation and is found by dividing the area of circular (circumferential) canals by the total vascular area (de Margerie, 2002). More specifically, they found that torsional loading causes a higher degree of laminarity (more circumferential canals), whereas, compression, tension or bending forces resulted in a lower degree of laminarity (more longitudinal canals). This pattern was further demonstrated in another study by de Margerie *et al.* where they examined how differences in torsional loading affect the vascular orientation within chicken humeri (de Margerie et al., 2005).

Most early studies in the fields of bone adaptation and bone strength focused on gross morphology, such as shape, size, mass, and trabecular arrangement due to the

visualization techniques available. With the advancement of high resolution imaging technology the internal microarchitecture of cortical bone has become increasingly accessible. In 2003, Cooper *et al.* demonstrated that it was possible to visualize and quantify human cortical porosity in three dimensions (3D) using desktop micro-computed tomography (micro-CT) (Cooper et al., 2003). Chapter 2 demonstrated that it is possible to visualize and quantify intracortical porosity in rats using desktop micro-CT (Britz et al., 2010) which had previously only been achieved using synchrotron radiation (SR) micro-CT (Matsumoto et al., 2006, Matsumoto et al., 2007). Desktop micro-CT is a far more accessible means by which to examine the effects of loading on bone adaptation from a different perspective – in 3D.

3.1.2 Study Objectives

To my knowledge there has not been an experimental study which has examined the effects of unloading on the 3D arrangement of the cortical canal network. Thus, the primary goal of this study was to employ desktop micro-CT technology to determine how loading affects the 3D orientation of cortical vascular canals (hereafter canals) in the rat using an immobilization (sciatic neurectomy) model.

3.2 Materials and Methods

3.2.1 Specimens

The left tibiae from ten Sprague-Dawley rats (30 weeks old) that had been immobilized (sciatic neurectomy) at three weeks of age for 27 weeks, right SHAM operated tibiae from these same rats (internal control) and the right tibiae from ten normal age-matched rats (external control) were utilized for this study. These specimens were

derived from the same animals as a previous study conducted on the femora by one of the co-authors (TJ) at the University of Tampere, Finland (Leppänen et al., 2010). Ethics approval for collection and study was granted by the Ethics Committee for Animal Experiments of the University of Tampere and the Provincial Government of Western Finland Department of Social Affairs and Health, Finland. For the current study approval was also granted by the University of Saskatchewan Biomedical Research Ethics Board for this research (permit #20080050; see appendix A). The rats were housed in cages (16 x 27 x 42 cm), two animals per cage, at 20 °C with a light cycle of 12 hours and had access to food and water *ad libitum*.

3.2.2 Micro-computed Tomography

Subsamples of the tibiae were cut using an Isomet 1000 slow speed saw (Buehler, Lake Bluff, USA) at the tibia-fibula junction and immediately distal to the tibial crest. This segment of bone was soaked in 3% hydrogen peroxide for three days to clear the soft tissue and allowed to air dry. These samples were scanned using a SkyScan 1172 (Kontich, Belgium) x-ray microtomograph (< 5 µm x-ray source spot size; 8.83 camera pixel size). As previously described in Chapter 2 of this thesis and in my 2010 publication (Britz et al., 2010), the samples were rotated through 360 degrees at a rotation step of 0.09 degrees. The x-ray settings were standardized to 100 kV and 100 µA, with an exposure time of 0.2 seconds per frame. Two-frame averaging was used to improve the signal-to-noise ratio. A 1 mm thick aluminum filter and a beam-hardening correction algorithm were employed to minimize beam-hardening artefacts. The scan time for each sample was approximately 3 hours. Each scan produced 1124 contiguous slices with a nominal resolution (isotropic voxel size) of 3 µm. To reduce image noise and preserve

detail in three dimensions, the image series were passed through a 3D median filter with a 3 x 3 x 3 cubic kernel. These images were analyzed using CT Analyzer 1.9.1.0 (SkyScan, Kontich, Belgium). The volume of interest contained the whole bone cross section and was extended through 300 slices (0.9 mm). The canals were identified using a standardized global threshold and the binarized datasets were then 'despeckled', removing noise in the form of 3D objects that consisted of less than 25 voxels. Percent porosity (canal volume fraction) and mean canal diameter were measured by methods described previously (Cooper et al., 2003). Briefly, canal diameter was measured using a model-independent distance transform based on Euclidean distance (see Jones et al., 2009, Mickel et al., 2008 for reviews) where the diameter at a specific point in the structure is the diameter of the largest sphere which can fit completely inside the 3D structure, which was first used to extensively measure trabecular thickness in bone (Hildebrand and Ruegsegger, 1997) and has since been used to measure canal diameter in cortical bone (Cooper et al., 2003). The measures of orientation were obtained by importing the micro-CT slices into Amira 5.3 (Visage Imaging Inc., Berlin, Germany) where a volume render of the canals was made (Figure 3.1A) and subsequently skeletonized (Figure 3.1B). Each skeletonized canal was divided into 30 pixel lengths (Figure 3.1C). To test whether a length of 30 pixels was adequate for measuring canal orientation the analysis was run at 15, 30 and 45 pixel lengths for one specimen (Figure 3.2). There were no differences between pixel lengths so I chose to use 30 pixels since it was roughly comparable to a 100 μm thick histologic section. The use of smaller segments for measuring canal orientation provided a more robust procedure since it took into consideration the non-linear (bent) canals. The angle of each canal segment was

measured with respect to the horizontal axis of the bone where an angle of 0° represents a radial canal and angles approaching +/- 90° are increasingly longitudinal. As I was interested in comparing radial versus longitudinal orientations, the absolute value of the angle was used to calculate mean orientation. Mean canal orientation was represented by a weighted average (by canal length) to account for those canal segments shorter than 30 pixels. This length-weighted average for canal orientation also provided a more robust measure of canal orientation that was capable of compensating for cases where the canals were broken up due to imaging limitations of the micro-CT. In addition to mean orientation, the orientations of the individual canal segments were used to calculate orientation distributions, binned in 5° intervals, for the whole sample. The plots of these distributions (Figure 3.3) provided a more in depth view of the differences underpinning the mean orientations. It should be noted that this study did not differentiate between primary and secondary vascular canals. It was assumed that the vascular canal network was dominated by primary canals since rats have a very low rate of remodeling and the study performed in Chapter 2 did not find any osteons in the ground sections (data not shown).

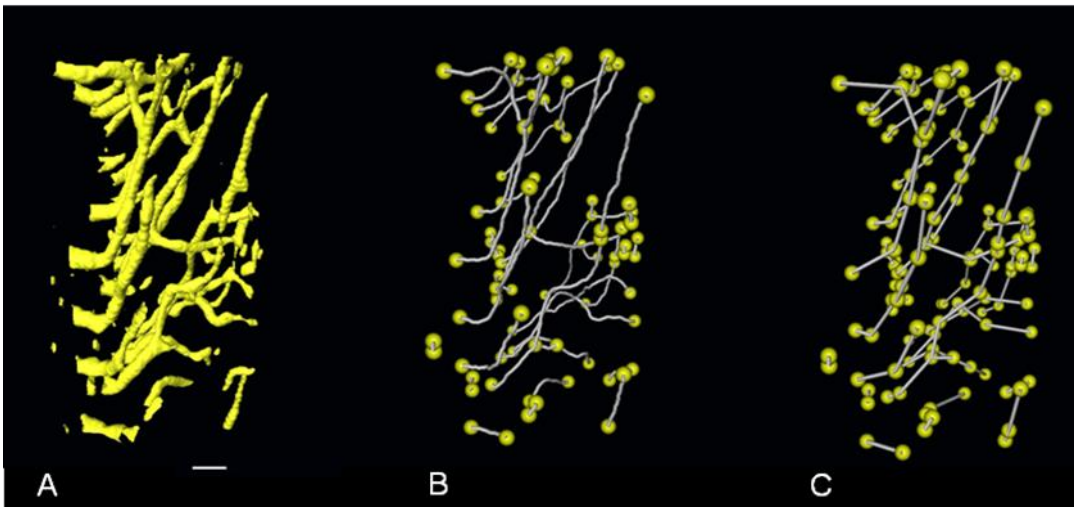

Figure 3.1 – A block of bone (300 micro-CT slices) from an immobilized bone showing the canals (A) the skeletonized canals with canal endpoints and branches highlighted (B) and the sub-sampled skeletonized canal structure at 30 pixel intervals with endpoints and branches highlighted (C). Scale bar = 100 μm.

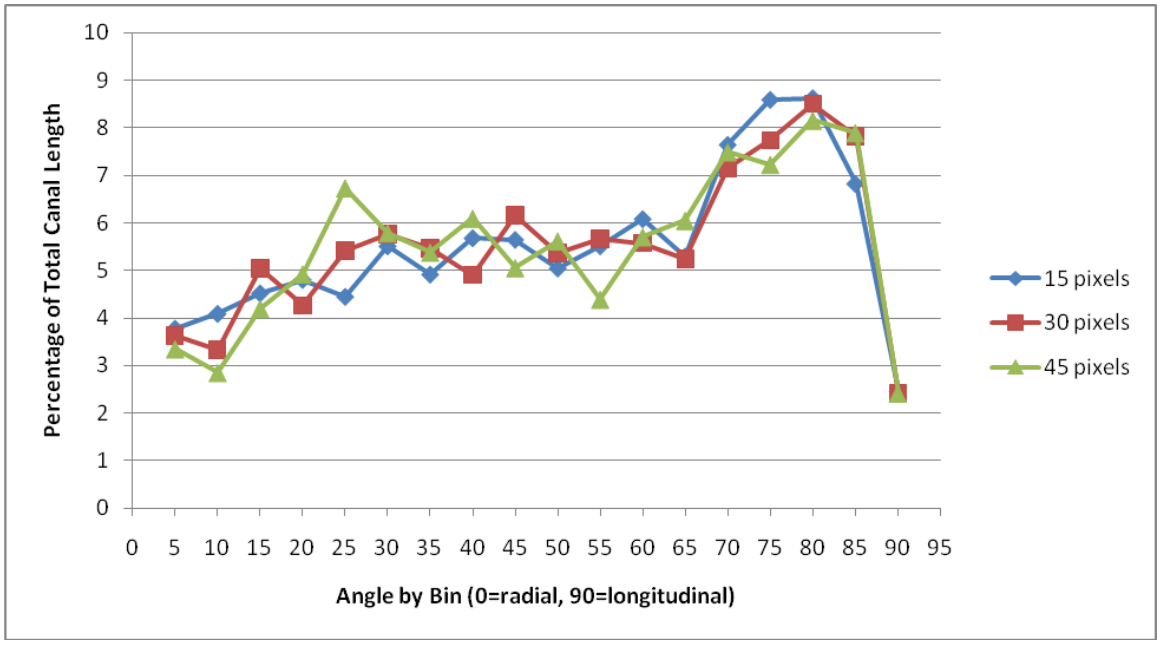

Figure 3.2 – Line graph showing the percentage of total canals within 5° bins for the whole bone for segmentation done at three different pixel lengths. Univariate analysis (general linear model) was employed to test for differences between the three segmentation lengths. This was followed by pair-wise post-hoc (Bonferroni) comparisons in the event a significant difference was found among the groups. No significant differences were found between any of the segmentation lengths.

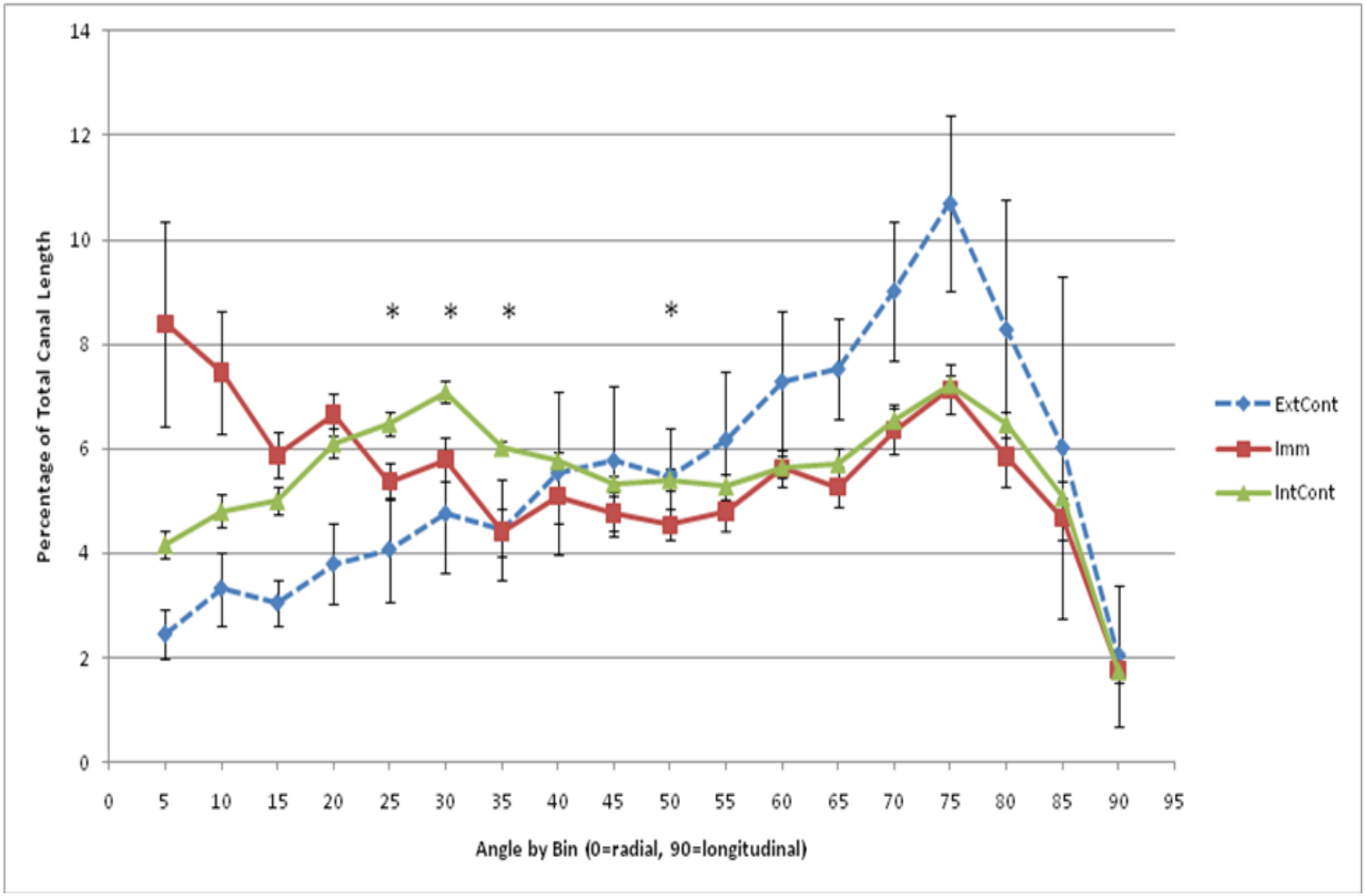

Figure 3.3 – Line graph showing the percentage of total canals within 5° bins for the whole bone of each group (external control, internal control and immobilized). The average of each bin from 10 specimens from each group are presented in this graph, where * represents $p<0.05$ for comparisons between the internal control and the immobilized bones using a paired t-test. The external control line is present for a visual comparison between the three different loading conditions. Error bars signify the standard error of the mean.

3.2.3 Statistical Methods

All statistical analysis was performed using SPSS 16.0 (SPSS Inc., Chicago, IL, USA). Univariate analysis (general linear model) was employed to test for differences in canal orientation, percent porosity, canal diameter, canal separation and body weight across the three groups. This was followed by pair-wise post-hoc (Bonferroni) comparisons in the event a significant difference was found among the groups. As the immobilized and internal groups were not truly independent, I also performed paired t-tests to compare all parameters for these two groups. Additionally, paired t-tests were performed on the 5° binned orientation results to further explore differences between the immobilized and internal control groups.

3.3 Results

Qualitatively there was a readily apparent difference in the cross-sectional shape of the immobilized bones. They were more circular with a thinner cortex, whereas, the external control and internal control bones were more triangular and had a thicker cortex (Figure 3.4). Summary statistics can be visualized in Figure 3.5. Mean canal orientation was found to be 51.3° in external control bones, 44.5° in internal control bones and 41.4° in immobilized bones. The general linear model revealed these values to be significantly different between external control and immobilized tibiae ($p<0.001$) and between the external control and internal control tibiae ($p<0.05$). In both cases the canals of the external control bones were oriented more longitudinally with mean differences of 9.9°and 6.8°, respectively. The difference between the immobilized and internal control tibiae was not significant using the general linear model or the paired t-test. When applied

to the binned orientation data the paired t-tests showed significantly ($p<0.05$) greater proportions of canals within 25°, 30°, 35°, and 50° bins of the internal control tibiae (Figure 3.3).

The mean percent porosity was 1.3%, 1.1% and 1.1% for immobilized, external control and internal control bones, respectively. Mean canal separation for these three groups was 178 µm, 180 µm and 160 µm, respectively. Mean body weight was found to be 304 g, 305 g and 304 g for these three groups, respectively. The general linear model found no differences between any of the groups for percent porosity, canal separation and body weight. With respect to canal diameter, the general linear model detected only one significant ($p<0.001$) difference with the immobilized tibiae having larger canals (17 µm) when compared to external control tibia (15 µm) (Figure 3.4). The canal diameter was 15 µm for both the internal control and external control tibiae.

Similarly, the paired t-test using mean results showed no significant difference between immobilized and internal control bones for percent porosity, canal separation, canal orientation or body weight. There were, however, significant differences found in canal diameter between these two groups ($p<0.001$).

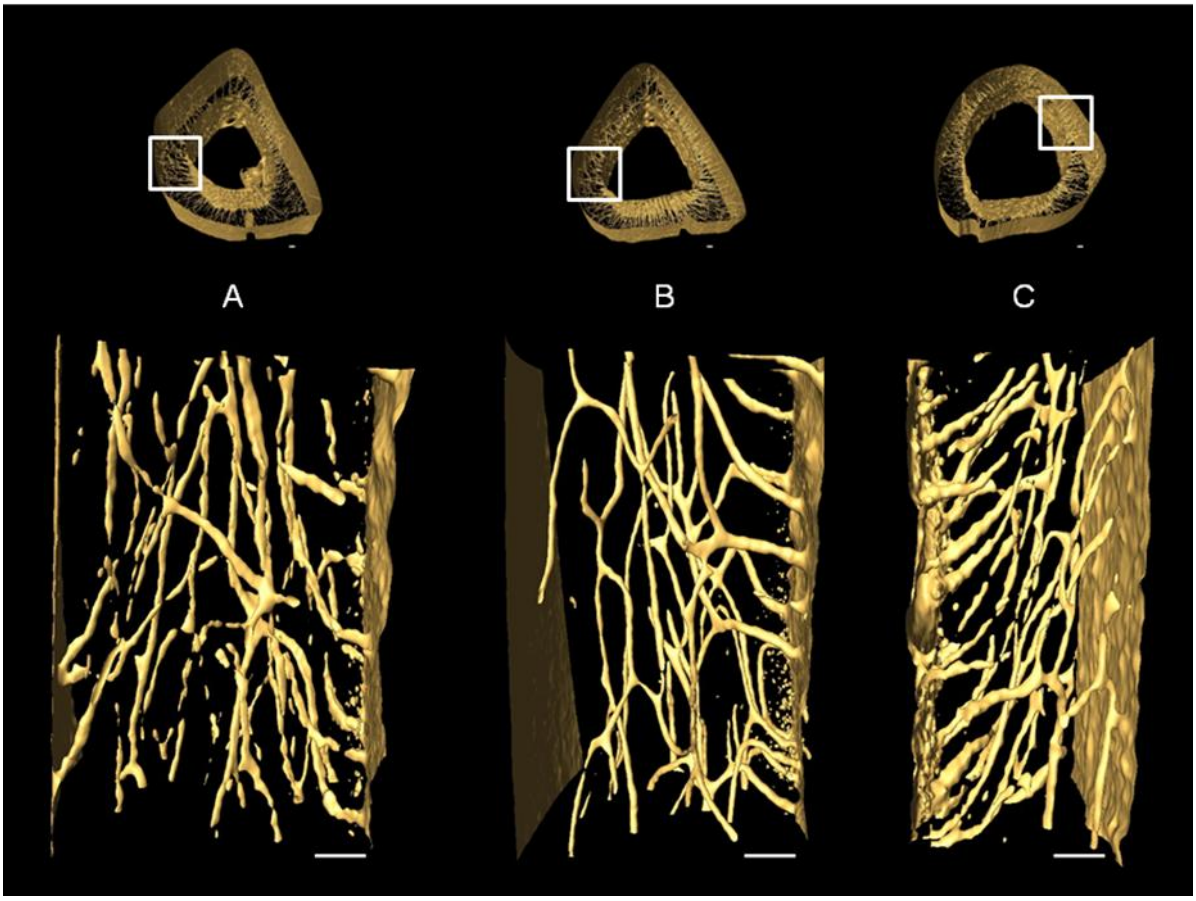

Figure 3.4 – Three dimensional renderings of 300 slices from longitudinal sections from the medial aspect of an external control bone (A) an internal control bone (B) and an immobilized bone (C). Keep in mind that both external and internal control bones are from the right limb (A and B) and the immobilized bone is from the left limb (C). Scale bar = 100µm.

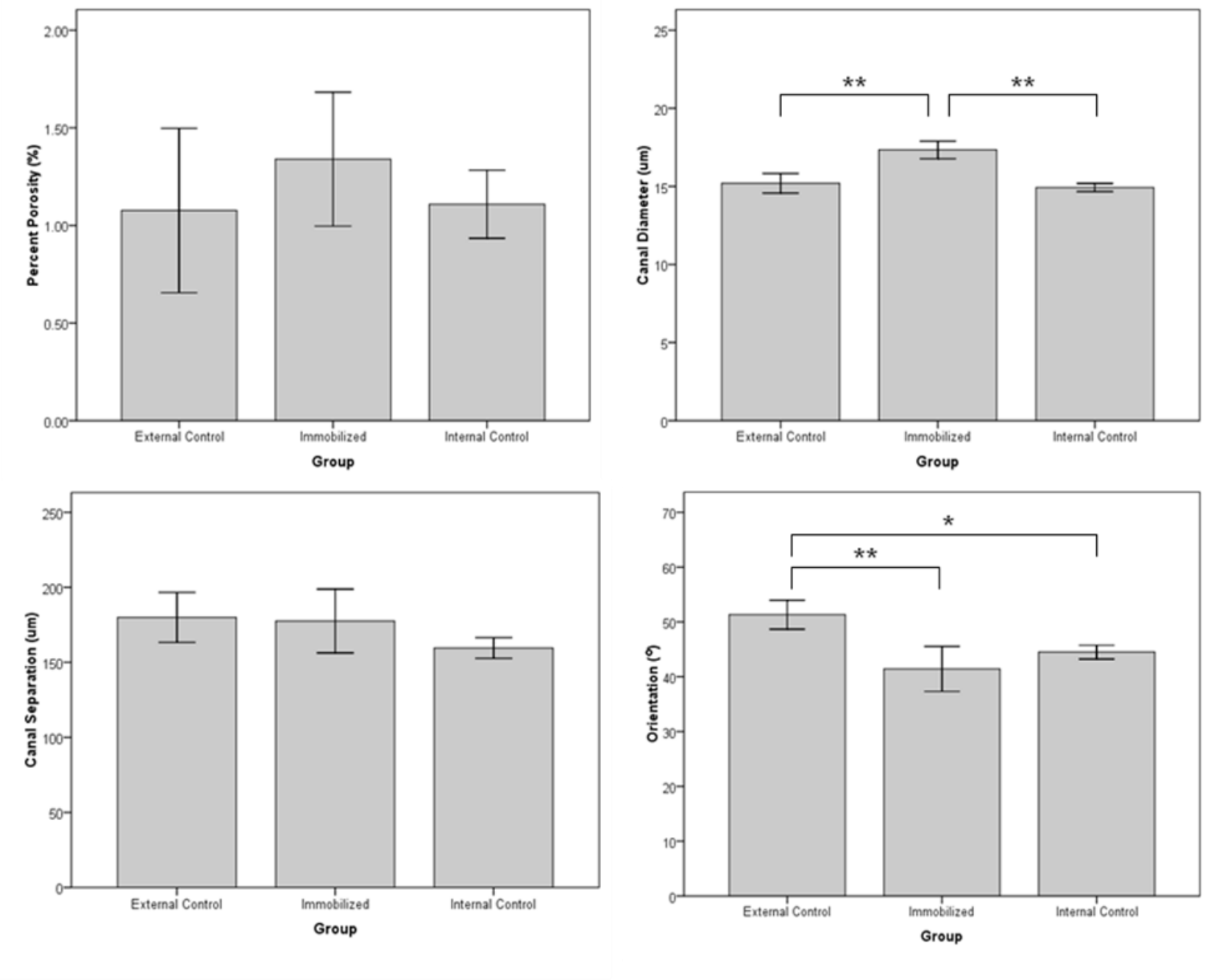

Figure 3.5 – Bar graphs for percent porosity, canal diameter, canal separation and orientation are represented here. Ten bones were analyzed for each of the three groups (external control, internal control and immobilize). Univariate analysis (general linear model) followed by pair-wise post hoc (Bonferroni) were performed and * represents $p<0.05$ and ** represents $p<0.001$. Error bars represent the 95% confidence interval.

3.4 Discussion

There have been numerous studies that look at the effect loading has on cortical bone morphology. More specifically, how loading affects cross sectional area (Bennell et al., 2002, Turner and Bell, 1986, Uhthoff and Jaworski, 1978), cortical bone porosity (Barth et al., 1992, Currey, 1988, Martin and Ishida, 1989, McCalden et al., 1993, Schaffler and Burr, 1988, Skedros et al., 1994a, Skedros et al., 1994b, Skedros et al., 1997, Steinberg and Trueta, 1981, Yeni et al., 1997), the canal network (Matsumoto et al., 2006, Matsumoto et al., 2007), osteon diameter (Britz et al., 2009, van Oers et al., 2008a, van Oers et al., 2008b, Young et al., 1986) and osteon orientation (Burger et al., 2003, Hert et al., 1994, Lanyon and Bourn, 1979, Petrtyl et al., 1996, Smit and Burger, 2000, Smit et al., 2002); however, to my knowledge none have experimentally examined how loading affects primary canal orientation in 3D. This study is thus the first of its kind to show in 3D that loading does affect cortical canal orientation during growth. Canals within the cortex of normally loaded bones (external controls) were oriented significantly more longitudinally (9.9° on average) than those found in immobilized bones ($p<0.001$) (Figure 3.4). Hert and Petrtyl's papers were the last to measure orientation; however, these measures were obtained using an India ink method with a focus on human secondary osteons (Hert et al., 1994, Petrtyl et al., 1996). They found that osteon orientation was relatively uniform, varying between 5° and 15° from the long axis of the bone (Hert et al., 1994). Hert *et al.* looked at vascular canals along with osteons, and described them as being 'longitudinally elongated meshes' (Hert et al., 1994). Another study by Pazzaglia and colleagues found that vascular canals (both primary and secondary) had a prevailing longitudinal orientation (Pazzaglia et al., 2010). Similarly, I

found that under normal loading conditions (external control group) primary vascular canals in the rat followed an oblique path which was significantly more longitudinal than both the immobilized and internal control limbs. While the *mean* orientation of the internal control limbs was not significantly different from the immobilized limbs, plots of the binned distributions of canal orientations (Figure 3.3) revealed that unloading was indeed having an impact. These plots had a peak at 70-75° in all groups, dominating the distribution of orientations for the external control group. In contrast, the immobilized group was characterized by higher numbers of more radially oriented canals, particularly those less than 15°. The internal control group exhibited an intermediate position between these extremes, with a bimodal distribution with its second peak at 25-30°. As Figure 3.3 demonstrates, this second peak resulted in significantly ($p<0.05$) higher percentages of canals in the 20-35° range when compared against the immobilized group.

The intermediate position for the internal control group is likely the consequence of altered loading due to compensation for the paralysis of the contralateral limb – a phenomenon known as the "crutch effect" (Dellon and Dellon, 1991, Malushte et al., 2004). Single limb nerve injury studies have found that the contralateral limb of rats undergoing this procedure encounter compensatory changes in the non-injured limb which are evident as a change in gait (Dellon and Dellon, 1991, Malushte et al., 2004) or dry bone weight (Cohen et al., 1999). This could explain both the difference I observed between the external and internal control groups as well as the lack of significance in mean orientation between the immobilized and internal control groups. The insignificant difference between the immobilized and internal control groups could be attributed to the systemic effects of the sympathetic nervous system. Sciatic neurectomy has been shown

to induce bone loss in the neurectomized limb, but also in the non-neurectomized contralateral limb (Kingery et al., 2003). This study showed that cross-talk between the contralateral limbs does occur; however, whether it is attributed to the sympathetic nervous system is heavily debated. Other studies looking specifically at cortical bone have found that innervated and denervated limbs react identically to controlled loading (de Souza et al., 2005, Hert et al., 1971), indicating the sympathetic nervous system does not modulate cortical bone gain induced by loading.

It is very rare that loading results in a uniform strain mode (Cooper et al., 2008). An example of this would be, in bending, when one side of the bone is under compression the opposite side will be under tension (Petrtyl et al., 1996). This regional variation in strain mode has been found to affect canal orientation (de Margerie et al., 2002). As such, the regional differences seen in Figure 3.4A and B may have been a result of the regional variation in strain mode. This may also explain why qualitatively there appeared to be less regional variation in canal orientation within the immobilized bones (Figure 3.4C). One of the limitations of this study was that regional variation of strain modes was not accounted for. I can make inferences in terms of what I would expect to see in terms of orientation by region based on what I know about regional strains in other bones. The rat tibia is a curved bone with its anterior aspect being convex and posterior aspect being concave, similar to that of a sheep radius. Studies looking at sheep radii have found that convex surfaces are strained in longitudinal tension, whereas, concave surfaces are strained in longitudinal compression (Lanyon and Baggott, 1976). I would expect to see more longitudinal canals in the anterior aspect of the rat tibia since it is under tension and Hert *et al*. have found that compression results in more oblique

osteons than tension does (Hert et al., 1994). I would also expect to find more radial canals in the medial and lateral aspects of the bone since the neutral axis should pass through these regions since it separates areas in compression from those in tension (Peterman et al., 2001, Sonoda et al., 2003). A study looking at canal orientation by region would confirm if this pattern would be observed and provide a better understanding of how loading is affecting bone microarchitecture and may shed further light on the distributions of canal orientations depicted in Figure 3.3.

Growth rate has been known to affect the primary microarchitecture of bone (Castanet et al., 1996, Castanet et al., 2000); however, a more recent study has shown that canal orientation is quite independent of growth rate (de Margerie et al., 2002). It has since been speculated that changes in canal orientation are more likely to reflect the bone's need to resist specific loads (de Margerie, 2002, Swartz et al., 1992). This is supported by my finding of different canal orientations in loaded versus unloaded bones. The predominant longitudinal orientation of the loaded bones in this study could be an adaptation to resist the shear stresses that are experienced by the tibia. The canals in the immobilized bones were more radial – suggesting this pattern arises in the absence of the stresses experienced during normal loading. The bones from the internal control group were significantly less longitudinal than the external control group but more longitudinal (difference not significant) than the immobilized bones. This may be due to a reduction in overall activity of the rats, causing the internal control limb as well as the immobilized limb to experience disuse. This coupled with the possibility of the internal control bone experiencing an altered loading condition due to the need to compensate for the loss of the contralateral limb's function (Dellon and Dellon, 1991, Malushte et al., 2004) could

explain why there is a difference between the external and internal control bones but not between the internal control and immobilized bones. Figure 3.3 supports the interpretation that such compensation did indeed affect the internal controls since their distribution of orientations was intermediate between that of the external control and the immobilized group.

If the differences in orientation I observed do indeed reflect a functional adaptation it would suggest some means of mechanosensation is utilized to control the incorporation of vasculature within bone during growth. Several studies have looked at the potential role of mechanosensation (e.g. based upon strain and fluid flow) in determining secondary osteon orientation (Burger et al., 2003, Smit et al., 2002, van Oers et al., 2008a); however, orientation of secondary structures is based upon the paths of osteoclastic cutting cones and thus represents a very different phenomenon. To my knowledge no study has looked at whether or not mechanosensation is a driving force behind primary canal orientation which is established as a bone grows. My experimental design did not allow us to look at the possible differences between growth rate and/or factors related to mechanosensation. A model to begin getting at 3D remodeling which is outlined in Chapter 4 will be important in assessing the degree to which these factors do or do not contribute to canal orientation.

Previously, it has been shown that loading has a positive effect on bone strength (Bagi et al., 1993, Bennell et al., 2002, Notomi et al., 2000, Raab et al., 1991, Verhaeghe et al., 2000). Experiments where the subjects were exercised found that exercise increased strength by changing bone geometry (cross sectional area), cortical bone thickness and area (Bell et al., 1980, Bennell et al., 2002, Järvinen et al., 2003a, Järvinen

et al., 2003b, Leppänen et al., 2008, Pajamaki et al., 2003, Woo et al., 1981). Microarchitectural changes within cortical bone such as, osteon area (Evans and Bang, 1967, Evans and Vincentelli, 1974), osteon density (Evans and Vincentelli, 1974, Vincentelli and Grigorov, 1985, Yeni et al., 1997) and intracortical porosity (Barth et al., 1992, Currey, 1988, Martin and Ishida, 1989, McCalden et al., 1993, Schaffler and Burr, 1988, Skedros et al., 1997, Yeni et al., 1997) were found to accompany these gross morphologic changes. More recently, canal orientation has been added to this list. Mullins *et al.* found that variation in canal orientation (Haversian and Volkmann canals) caused up to a 20% decrease in longitudinal shear modulus, and therefore bone strength (Mullins et al., 2007). Bone strength testing was not within the scope of the present study; however, according to the aforementioned study by Mullins *et al*., I would expect that immobilized bones would be weaker than external control bones due to their differing canal orientations (Mullins et al., 2007).

These results revealed that loading affects the 3D orientation of vascular canals within rat cortical bone. This could contribute, at least in part, to the positive effect loading has on bone strength (Bagi et al., 1993, Bennell et al., 2002, Notomi et al., 2000, Raab et al., 1991, Verhaeghe et al., 2000). I also found there to be a significant difference in canal diameter between external control and immobilized bones and internal control and immobilized bones. The literature suggests that canal diameter may also affect bone strength (Sevostianov and Kachanov, 2000, Yeni et al., 1997). Whereby, larger canals cause the bone to be weaker. My results indicate that cortical bone in the rat has a highly variable microarchitecture which is directly affected by mechanical stimuli. I hypothesize

that the variation in cortical bone microarchitecture reflects a functional adaptation aimed at improving bone's ability to endure loading.

3.5 Conclusion

The finding that loading affects canal orientation has implications for studies focusing on the mechanical properties of bone, and will ultimately lead to advancements in the understanding of bone adaptation, aging and disease. This study also opens the door for subsequent studies looking at the effect of regional variation on primary vascular canal measures, especially 3D orientation, due to differential strain modes. Further studies are also needed to clarify whether mechanotransduction and/or growth rate is the primary determinant of canal orientation. The next chapter of this thesis looks at inducing remodeling in rats, making them a better model for future studies looking at loading and secondary canal orientation.

CHAPTER 4:

DEVELOPMENT OF A RAT MODEL TO STUDY THE 3D REGULATION OF CORTICAL BONE REMODELING: A PILOT STUDY

4.1 Introduction

Chapter 3 demonstrated that loading affects primary vascular canal orientation; however, I was unable to assess how loading affects remodeling events (secondary vascular canals) since rats have such a low rate of remodeling. This chapter looks at different ways to induce remodeling in the rat through pregnancy, lactation and calcium restriction. More specifically, it examines whether calcium restriction alone is adequate to induce remodeling or if pregnancy and lactation are needed to increase the body's demand for calcium in order to initiate bone resorption and therefore remodeling. Once a technique for inducing remodeling in rats is established it can be employed for looking at how loading and other stimuli affect the orientation of these remodeling events (BMUs). It should be noted that subsequent referrals to BMUs are referring to those related to secondary osteon formation.

4.1.1 Bone Remodeling

Remodeling produces secondary structures within cortical and trabecular bone and is the primary process of skeletal renewal and functional adaptation in mature bone. Remodeling removes and replaces small packets of bone through the initiation of BMUs. A BMU contains two main cell types 1) osteoclasts which resorb bone, forming what is known as a resorption space (Robling et al., 2006) and 2) osteoblasts that fill in the resorption space with osteoid which mineralizes to form new bone (Robling et al., 2006).

This process results in the formation of an osteon (including a centrally located secondary vascular canal) or hemi-osteon in cortical or trabecular bone, respectively.

The concept that bone renews itself throughout life by remodeling has been accepted since the 1800's (Tomes and de Morgan, 1853); however, the factors that activate a BMU are still not well characterized, but appear to include mechanical and hormonal stimuli (Parfitt, 2002, Pearson and Lieberman, 2004). Advancements have been made in understanding how the cellular activity of a BMU is regulated (Teitelbaum, 2000); however, little was known regarding the 3D morphology of BMUs and the osteons they produce until Cooper *et al.*'s study in 2006 looking at BMUs in human cortical bone using micro-CT (Cooper et al., 2006). The ability to image BMUs in 3D provides researchers with a new perspective in which to understand how BMUs are regulated. More specifically, how mechanical stimuli affect BMU orientation and morphology.

Imaging technology is constantly evolving and has advanced to the point where rat vascular canals can be imaged and quantified using a desktop micro-CT as previously described in Chapter 2 and my 2010 publication (Britz et al., 2010) and osteocyte lacunae can be imaged in mice using nano-CT (Schneider et al., 2007, Voide et al., 2009). The caveat of these high resolution imaging techniques is the decrease in the size of the field of view (Cooper et al., 2007b, Schneider et al., 2007). In order to overcome the small field of view in these new imaging techniques small animal models are needed to address questions regarding how different stimuli affect BMUs, more specifically, mechanical stimuli. The aforementioned studies have indicated that rats and mice have bones that are small enough to utilize these new 3D imaging techniques for imaging their bone micro- and ultrastructure (vascular canals and osteocyte lacunae, respectively). The use of rodent

bones in studies regarding BMU characteristics and therefore remodeling have their own limitations. Unlike bones of higher mammals, rodent bones rarely undergo intracortical remodeling (Schneider et al., 2007) so before they can be used to test remodeling hypotheses the remodeling events in question must be induced.

4.1.2 Inducing Remodeling in Rats

There are two non-pharmacological ways by which to induce remodeling within the rat that are commonly used 1) introduction of an exercise program (increased loading) and 2) pregnancy and lactation (increased calcium demands). Long bones respond to physiologic changes that occur during exercise. For example, there are increases in bone perfusion during exercise (Tondevold, 1983, Tondevold and Bulow, 1983). Literature suggests that different forms of exercise can induce intracortical remodeling in rats (Li et al., 1991, Notomi et al., 2000, Parker, 1977); however, the magnitude of this change is dependent on the intensity of the exercise (Antonov, 1980). Inducing intracortical remodeling through exercise does not provide a good solution to the lack of remodeling within the rat model since there is extensive debate as to whether or not remodeling occurs to repair microcracks (Martin, 2002). This provides a major problem in using this technique for studies looking at how mechanical stimuli affect BMU orientation since the exercise regime could be damaging the bone, forming microcracks, which would then drive the orientation of the BMUs (Martin, 2003).

Intracortical remodeling can also be induced in rats through the natural processes of pregnancy and lactation (Ellinger et al., 1952, Ream et al., 1983). It is well known that the skeleton serves as a store of calcium, and during periods of lactation rats lose calcium from their bones regardless of the amount of calcium in their diet (Komarkova et al.,

1967, Spray, 1950). During a normal lactation period in rats, there may be as much as a 35% loss of skeletal bone mineral during the 21 days of lactation (Brommage and DeLuca, 1985). It has been shown that this loss of skeletal bone mineral during lactation is met through bone resorption (Ellinger et al., 1952).

A variety of experiments have been conducted that look at the effects of pregnancy and lactation (Miller et al., 1986, Vajda et al., 2001), multiple pregnancies and lactations (Miller and Bowman, 2004) and pregnancy and lactation on a calcium restricted diet (Lozupone and Favia, 1988, Rasmussen, 1977a) on bone microstructure and have found evidence of remodeling being induced by these techniques. The justification for conducting these tests with a calcium restricted diet is that with a calcium deficient diet, pregnancy and lactation may cause greater decrease in bone mineral (Bawden and McIver, 1964, Rasmussen, 1977b) which may be achieved through an increase in the number of remodeling events.

4.1.3 Pilot Study Objectives

Inducing intracortical remodeling through pregnancies, lactations and calcium restrictions present a more natural way to look at the effects mechanical stimuli have on remodeling. It is a more effective solution to the low levels of intracortical remodeling because it does not produce 'side effects' such as microcracks, which may influence BMU orientation. Thus, the primary goal of this pilot study was to compare the levels of remodeling induced by either calcium restriction alone or coupled with pregnancy and lactation.

4.2 Materials and Methods

4.2.1 Specimens

Four female Sprague-Dawley rats (19 weeks old) were separated into two groups 1) calcium restricted (n=2) 2) calcium restricted while going through pregnancy and lactation (n=2). These two groups were fed a diet containing 0.05% calcium (TD.10908, Harlan Laboratories Inc.) for the duration of the study. The females in the pregnancy and lactation while on a calcium restricted diet group were mated with age matched male Sprague-Dawley rats (n=2) at 20 weeks of age. At the end of the reproductive cycle the rats were euthanized (26 weeks old) by carbon dioxide exposure followed by cervical dislocation. The left tibiae from these rats were extracted and employed for this study. Approval for this pilot study was granted by the University of Saskatchewan Biomedical Research Ethics Board (permit # 20100097; see appendix A). The rats were housed in pairs in conventional cages, at 20-22°C and had access to food and water *ad libitum*.

4.2.2 Micro-computed Tomography

Subsamples of the tibiae were cut using an Isomet 1000 slow speed saw (Buehler, Lake Bluff, USA) at the tibia-fibula junction and immediately distal to the tibial crest. This segment of bone was soaked in 3% hydrogen peroxide for three days to clear the soft tissue and allowed to air dry. These samples were scanned using a SkyScan 1172 (Kontich, Belgium) x-ray microtomograph (< 5 µm x-ray source spot size; 8.83 camera pixel size). As previously described in Chapter 2 and my 2010 publication (Britz et al., 2010), the samples were rotated through 360 degrees at a rotation step of 0.09 degrees. The x-ray settings were standardized to 100 kV and 100 µA, with an exposure time of 0.2 seconds per frame. Two-frame averaging was used to improve the signal-to-noise ratio. A

1 mm thick aluminum filter and a beam-hardening correction algorithm were employed to minimize beam-hardening artefacts. The scan time for each sample was approximately 3 hours. Each scan produced 1124 contiguous slices with a nominal resolution (isotropic voxel size) of 3 μm. To reduce image noise and preserve detail in three dimensions, the image series were passed through a 3D median filter with a 3 x 3 x 3 cubic kernel. These images were analyzed using CT Analyzer 1.9.1.0 (SkyScan, Artselaar, Belgium). The volume of interest contained the whole bone cross section and was extended through 300 slices (0.9 mm). The canals were identified using a standardized global threshold and the binarized datasets were then 'despeckled', removing noise in the form of 3D objects that consisted of less than 25 voxels. Cortical thickness was measured using a model-independent distance transform based on Euclidean distance (see Jones et al., 2009, Mickel et al., 2008 for reviews) where the diameter at a specific point in the structure is the diameter of the largest sphere, which can fit completely inside the 3D structure. BMU counts were obtained by importing the micro-CT slices into Amira 5.3 (Visage Imaging Inc., Berlin, Germany) where a volume render of the canals was made and the BMU's (blunt ended canals) were manually counted and verified in ImageJ (v1.43, NIH; http//rsb.info.hih.gov/ij/) (Figure 4.1). Bone volume was also measured within Amira and used to calculate BMU density (number of BMUs per volume of bone; BMU/mm^3).

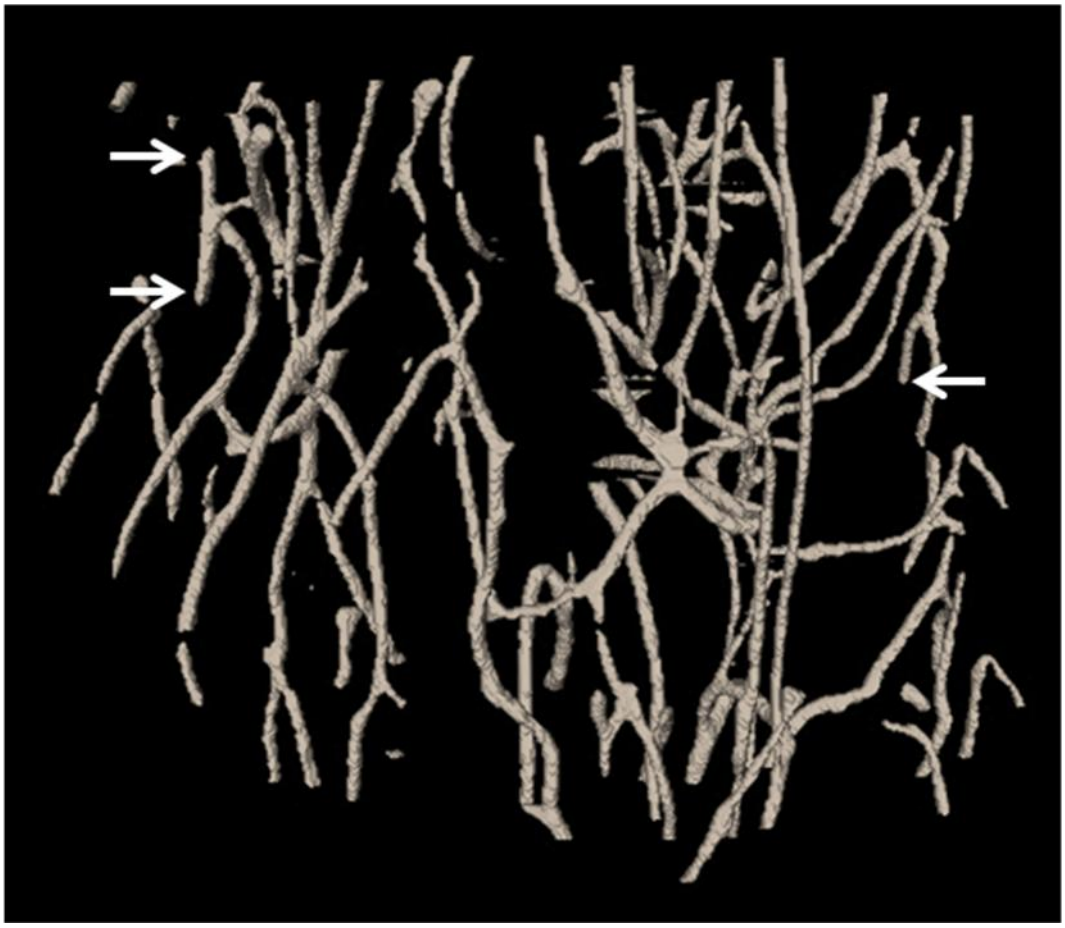

Figure 4.1 – A 3D rendering of the blunt ended canals counted in this study from the anterior region of the cross section. The arrows are indicating a few of the blunt ends. Scale bar = 100 μm.

4.3 Results

Due to the nature of this pilot study, there were only two specimens per group; therefore, no statistical tests were performed making this a qualitative study. All measures can be seen in Table 4.1. The rats that were just on the calcium restricted diet (469 g and 437 g) seemed to weigh more than those that were subjected to pregnancy and lactation (360 g and 323 g). No behavioral changes were noted, other than late in pregnancy the pregnant rats moved around less than their non-pregnant counterparts. Another point worth noting was that Rat 1 in the pregnancy and lactation group had 12 pups whereas, Rat 2 had 15. Qualitative observations of the cross sections revealed a marked difference in cortical thickness between the two groups (Figure 4.2). Mean cortical thickness for the calcium restricted rats and the pregnant and lactating rats that were on a calcium restricted diet were 622 μm and 419 μm, respectively. The rats that were subjected to just the calcium restriction seemed to have thicker cortices then those who also underwent pregnancy and lactation (Figure 4.2). The calcium restricted rats had a mean BMU count of 16 where as the rats that had also underwent pregnancy and lactation had a mean BMU count of 13 BMUs. Due to the similarity in BMU counts for both groups the number of BMUs per bone volume (BMU density) was measured. Mean BMU density was found to be 4.0 BMUs/mm^3 for the calcium restricted rats and 5.5 BMUs/mm^3 for the rats that experienced pregnancy and lactation as well. It should also be noted that there seemed to be large resorption spaces, which are more consistent with BMUs found only in the pregnant and lactating group (Figures 4.3 and 4.4).

Table 4.1 – Measures taken for each specimen in this pilot study.

Measure	Calcium Restriction		Calcium Restriction, Pregnancy and Lactation	
	Rat 1	*Rat 2*	*Rat 1*	*Rat 2*
Body Weight (g)	437	469	360	323
Cortical Thickness (μm)	641	603	388	450
Number of BMUs	13	19	14	12
BMU Density (BMU/mm^3)	3	5	6	5

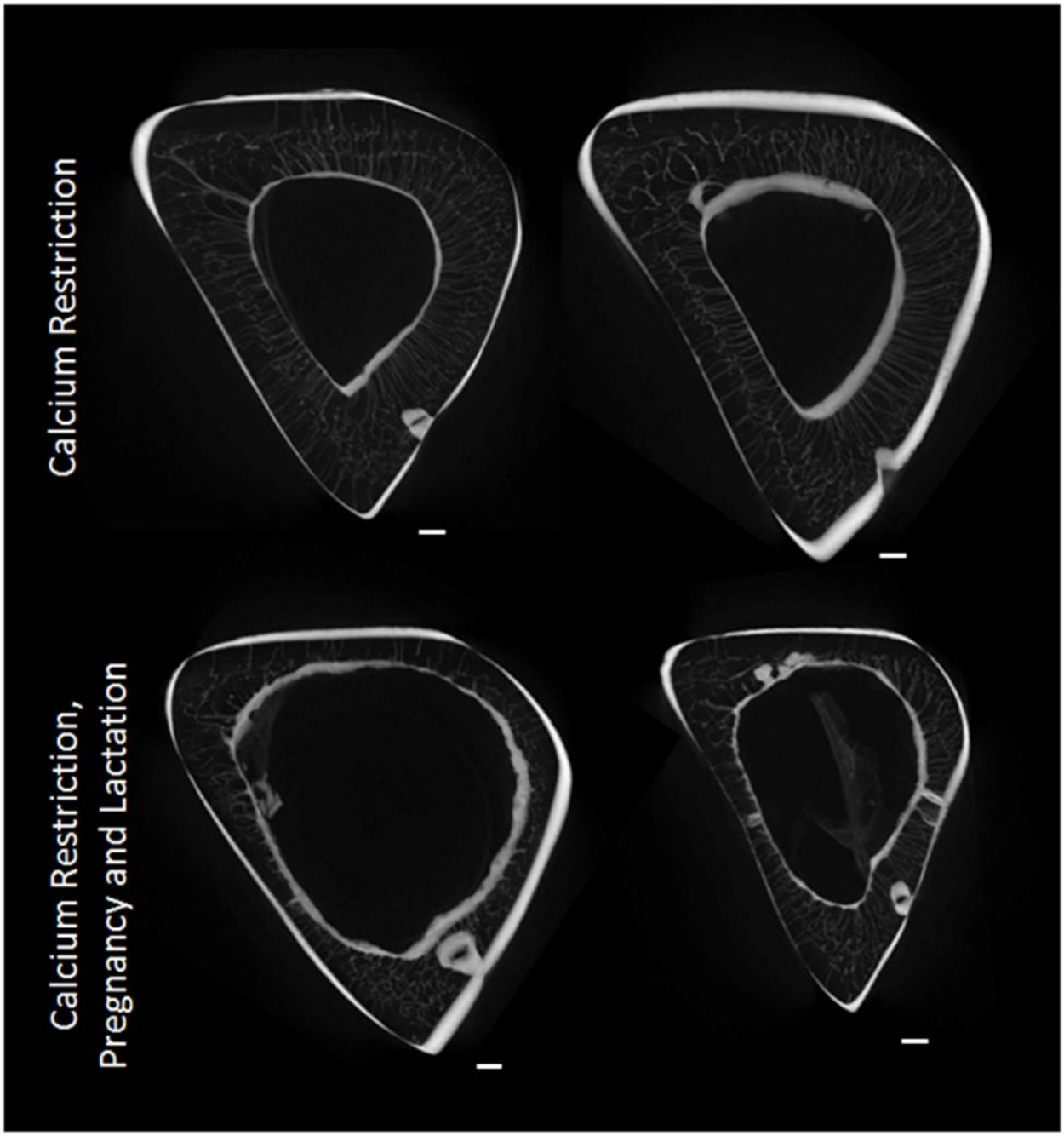

Figure 4.2 – Standard deviation projections through 300 micro-CT slices for each of the bones employed in this study. Note the differences in cortical thickness. With regards to Table 4.1 – Rat 1 for both groups is on the left and Rat 2 is on the right. Scale bars = 100 µm.

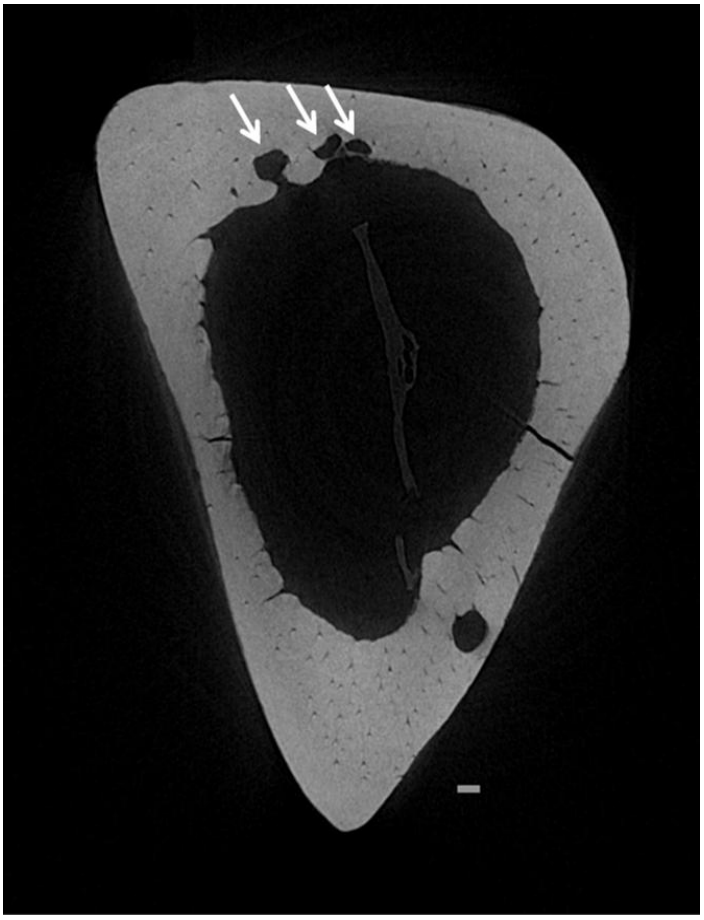

Figure 4.3 – A micro-CT slice from a femur of a rat that went through pregnancy and lactation while on a calcium restricted diet. The white arrows indicate resorption spaces. Scale bar = 100 µm.

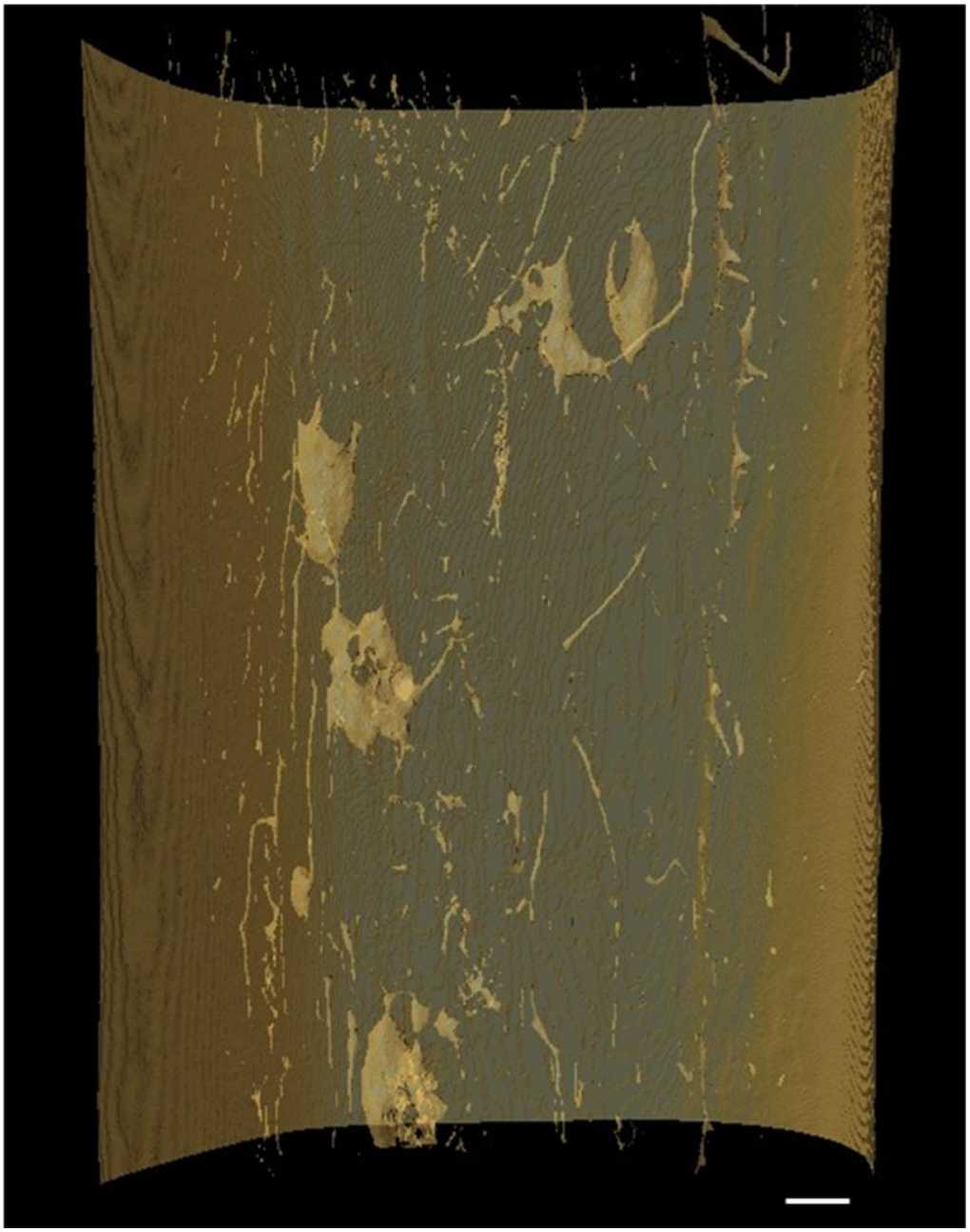

Figure 4.4 – A 3D rendering of the resorption spaces seen in Figure 4.3 and some of the surrounding canals. Scale bar = 100 µm.

4.4 Discussion

It has been previously noted that different combinations and durations of calcium restriction, pregnancy and lactation induce remodeling in rat cortical bone (Currey and Hughes, 1973, de Winter and Steendijk, 1975, Ellinger et al., 1952, Leopold et al., 1995, Lozupone and Favia, 1988, Miller and Bowman, 2004, Rasmussen, 1977a, Ream et al., 1983, Ruth, 1953); however, to my knowledge a comparative study between methods of induction has never been conducted looking specifically at BMU or osteon numbers. This pilot study is thus the first of its kind to examine how calcium restriction, pregnancy and lactation affect BMU numbers as well as the gross morphology of the bone (cortical thickness). Bones subjected to pregnancy and lactation while on the calcium restricted diet seemed to have thinner cortices then those on the calcium restricted diet alone (Figure 4.2). Rasmussen found that rats fed a calcium restricted diet had thinner cortices than rats fed a normal diet and that rats that went through pregnancy and lactation while on a calcium restricted diet had the thinnest cortices out of the three groups (Rasmussen, 1977a) which is in agreement with what was seen in this pilot study.

The BMU counts for the calcium restricted rats seemed to be more variable than those obtained from the rats that had also undergone pregnancy and lactation (Table 4.1), which demonstrates the inherent limitation of this pilot study – inadequate number of specimens. The small number of specimens permitted to be used in this study did not allow for possible inter-individual variation which is evident in the shape difference seen in Figure 4.2 between the two pregnant and lactating rats, and is possibly responsible for the similarity in the BMU counts for the two groups. It was not possible to overcome this limitation by comparing the results from this pilot study to other studies which indicate

remodeling is induced in rat cortical bone since BMU or osteon counts were not made in these studies, large resorption spaces or osteons were just noted as being seen (Currey and Hughes, 1973, de Winter and Steendijk, 1975, Ellinger et al., 1952, Leopold et al., 1995, Lozupone and Favia, 1988, Miller and Bowman, 2004, Rasmussen, 1977a, Ream et al., 1983, Ruth, 1953).

Since there seemed to be differences in cortical thickness between the techniques used to induce remodeling in this study, the use of a BMU count for each bone may not be indicative of which technique is more apt to induce remodeling. For this reason, BMU densities (number of BMUs per mm^3 of bone) were calculated. The BMU densities seemed to be similar between the two groups (Table 4.1). A possible explanation for this is that resorption spaces indicative of remodeling events tend to be seen on the endosteal side of the cortex (de Winter and Steendijk, 1975, Leopold et al., 1995, Lozupone and Favia, 1988), so the increased endosteal resorption resulting in the thinner cortices of the pregnant and lactating rats in this pilot study could be eliminating potential BMUs. Other studies have found that the administration of a calcium restricted diet to rats undergoing pregnancy and lactation results in a greater decrease in cortical thickness than the processes of pregnancy and lactation alone (de Winter and Steendijk, 1975, Lozupone and Favia, 1988). This finding indicates that pregnancy and lactation alone could provide a better model for inducing remodeling events since there is a reduction in the amount of endosteal resorption, thereby fewer potential BMUs are being eliminated due to endosteal resorption.

It must be noted that the BMU counts in this pilot study should not be viewed as exhaustive. Since the cortical canal network is complex and highly variable it is likely not

all BMUs were detected. Additionally, BMUs were counted by determining the number of blunt ended canals; however, these were of the same magnitude as the rest of the vasculature within the cortex. Blunt ended canals normally indicative of BMUs tend to be enlarged compared to the surrounding vascular canals (Cooper et al., 2006). This poses the question of whether or not these blunt ended canals are actually due to remodeling. Normally, remodeling employs the activation of multiple osteoclasts, resulting in an enlarged blunt end (cutting cone); however, a recent study by Nango *et al*. suggests that remodeling in mice may be initiated by a single osteoclast (Nango et al., 2010). This would explain why the blunt ended canals in this study were the same size as the surrounding vascular canals. Large resorption spaces which are indicative of 'normal' (multi-osteoclast) remodeling were seen in the rats that experienced pregnancy and lactation (Figures 4.3 and 4.4). This observation suggests rodents may undergo two forms of remodeling. It is possible that rats have very low calcium demands normally so boring a large resorption space in their cortex for adaptation purposes alone would be uneconomical and potentially disastrous to the bone in terms of strength and viability. Whereas, single osteoclast resorption could provide the bone adaptation needed for the bone to endure the mechanical strains it experiences and enough calcium to meet their nutritional demands without severely weakening the bone. If rats do actually have two forms of remodeling, many of the canals considered to be primary in Chapter 3 might actually be secondary canals.

The results of this pilot study indicate that intracortical remodeling can be induced in rats; however, due to sample size it is inconclusive as to whether or not calcium restriction alone is sufficient to induce remodeling to a point where it provides an

appropriate model for using rats in bone adaptation studies. The rats that underwent pregnancy and lactation seemed to have larger resorption spaces indicative of traditional BMUs making it the better technique for inducing remodeling; however, it is possible that rats undergo two forms of remodeling. This warrants further study into the mechanisms by which rat bones remodel and a larger scale comparative study of techniques for inducing remodeling in rats.

4.5 Conclusion

It is possible to induce remodeling in rat cortical bone; however, this study was inconclusive as to whether calcium restriction alone provides a significant increase in remodeling sufficient to ensure the rat is an appropriate model for bone adaptation studies. This pilot study has also demonstrated the possibility that rats undergo two forms of remodeling which could pose a further limitation in the use of rats for bone adaptation studies in terms of interpolating the results from these studies to questions of bone adaptation in humans.

CHAPTER 5:

CONCLUSION

5.1 Introduction

The overarching goal of this thesis was to contribute to the greater understanding of the 3D microarchitecture of cortical bone and how it adapts to mechanical stimuli. Relative to the knowledge of how loading affects bone gross morphology and trabecular arrangement, little is known regarding 3D cortical microarchitecture. This is, in part, due to the recent availability of high resolution imaging techniques and their inherent limitations, such as the trade-off between resolution and field of view (Cooper et al., 2007a, Schneider et al., 2007). Therefore, a small animal model is needed to overcome this imaging limitation as well as provide a model that can be experimentally manipulated to address hypotheses concerning bone's ability to adapt to mechanical stimuli. This, in turn, will contribute to a number of research fields including bone biology and disease, paleontology and physical anthropology.

5.2 Overview

The study presented in Chapter 2 laid the foundation for the thesis in terms of methodology. The scanning protocol developed in this chapter allowed for the visualization and quantification of the vascular canals within rat cortical bone using a desktop micro-CT. Previously, rat cortical porosity had only been examined in 3D using SR micro-CT (Matsumoto et al., 2006, Matsumoto et al., 2007). It was found that desktop

micro-CT provides a reliable measure of percent porosity and a correctable measure of canal diameter (desktop micro-CT overestimates this measure by 5 microns).

Chapter 3 presented, to my knowledge, the first study to measure the 3D orientation of vascular canals within rat cortical bone. The scanning protocol developed in Chapter 2 was employed to generate the 3D data sets needed to measure orientation. This chapter examined the impact of immobilization (unloading) on cortical vascular canal orientation within the rat tibia. I found that loading affects cortical canal orientation during growth. Under normal loading conditions (external control group) primary vascular canals in the rat followed an oblique path, which was significantly ($p<0.001$) more longitudinal than both the immobilized and internal control groups (9.9° and 6.8°, respectively). The mean orientation of the internal control group was not significantly different from the immobilized group, plots of the binned distributions of canal orientations revealed that loading was having an impact, and that mean orientation does not provide a representative measure of how loading is affecting the orientation of vascular canals around the diaphysis.

Chapter 4 was a pilot study, which explored different methods for inducing cortical bone remodeling in the rat tibia. The ability to do this would make rats a better model for future studies looking at loading and canal orientation. This chapter compared calcium restriction and calcium restriction coupled with pregnancy and lactation in terms of cortical thickness, number of BMUs and BMU densities. Pregnancy and lactation coupled with calcium restriction seemed to result in bones with thinner cortices than those that were subjected to calcium restriction alone. There did not appear to be any differences between the two groups for number of BMUs and BMU densities; however

there were only two specimens per group, which did not allow me to account for inter-individual variation or perform statistical analyses. This chapter also demonstrated the possibility that rats undergo two forms of remodeling (single and multi-osteoclast resorption); however, it should be noted that the large resorption spaces were only observed in the rats that had been subjected to pregnancy and lactation in combination with being fed a calcium restricted diet.

5.3 Future Directions

With respect to the original purpose of this thesis, a larger scale follow up of the study presented in Chapter 4 is needed before an experimental test of how loading affects the 3D orientation of remodeling events can be executed. With regards to this follow up study, I think it would be useful to look at the effects of calcium restriction, pregnancy and lactation at different time points to maximize the number of BMUs while minimizing endosteal resorption. Since accumulation of bone mineral has been associated with pregnancy (Miller et al., 1986) looking at different time points during lactation may prove more advantageous in terms of maximizing BMU densities. During normal lactation in rats, there may be as much as 35% loss of skeletal bone mineral during the 21 days (Brommage and DeLuca, 1985). This suggests that there would be less endosteal resorption earlier in lactation. Examining the cortical bone microarchitecture after one, two and three weeks of lactation would allow for a better understanding of when and where this loss of bone mineral is occurring. It would also allow for the optimization of BMU densities, therefore, providing an effective technique for inducing remodeling in rat cortical bone. Another solution to the extensive endosteal resorption that occurs during

pregnancy and lactation, especially on a calcium restricted diet, would be to examine different skeletal elements that either have no medullary cavity or a smaller one. The absence of a medullary cavity would force the bone to remodel in order to obtain the body's calcium requirements instead of focusing primarily on resorbing the endosteal surface (Figure 5.1).

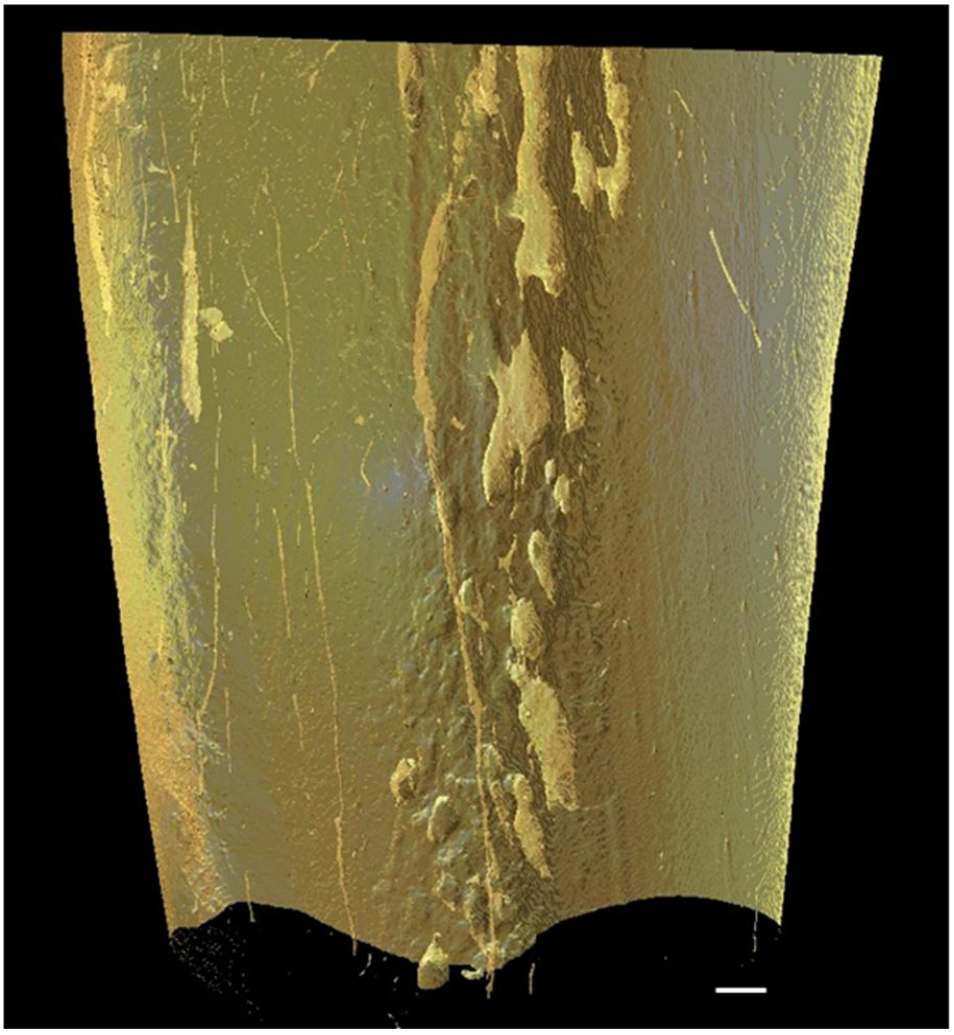

Figure 5.1 – A 3D rendering of the BMUs found in the mid-diaphysis of a rat ulna. The ulna was from one of the rats employed in Chapter 4 who was subjected to pregnancy and lactation while on a calcium restricted diet. Scale bar = 100 µm.

Before further studies can be performed looking at how loading affects the orientation of remodeling events a better understanding of how rats remodel is needed. Chapter 4 addressed the possibility of rats having two processes of remodeling, single and multi-osteoclast remodeling. The hypothesis of two modes of remodeling could be tested in two ways 1) section the tibia from the study described in Chapter 4 at the tip of the 'cutting cone' (blunt end) for both the small and larger remodeling events and stain for osteoclasts 2) perform a study similar to that described in Chapter 4 and use in vivo micro-CT to track the remodeling events. While both experiments have their merits they both have their limitations as well. Using histology to count the number of osteoclasts at the tip of the 'cutting cone' would indicate whether resorption was due to one or multiple osteoclasts; however, obtaining a section right at the tip would be difficult even with using the micro-CT scans for reference points. Using in vivo micro-CT to track remodeling events would allow for the examination of what is happening during the remodeling process. More specifically, are the bigger resorption spaces seen in the rats that were subjected to pregnancy and lactation while being on a calcium restricted diet due to a different mode of remodeling or are they formed by coalescing remodeling events? The average diameter of these larger resorption spaces was 125 μm, which is larger than the diameter of an osteon (72 ± 14 μm) found in rat cortical bone (Jowsey, 1966). This would suggest that the larger resorption spaces are not the product of a single remodeling event.

The use of in vivo micro-CT is a novel technique for tracking these remodeling events, the caveat being the radiation dose experienced by the rat during the scans. Desktop in vivo micro-CT systems have primarily been used to examine trabecular bone

structure (Boyd et al., 2006, Campbell et al., Waarsing et al., 2004). This is due to the resolution capabilities of the system. Most in vivo micro-CT scanners are only able to get down to a 10 μm voxel size, which is not able to discern and quantify vascular canals within rat cortical bone. The problem with increasing resolution is the inadvertent increase in radiation dose that accompanies this change due to the longer scan times required (Ford et al., 2003). SR micro-CT could provide the solution to this resolution limitation inherent of desktop systems since synchrotron radiation improves image quality, reduces scan time and enables higher resolutions (Peyrin, 2009). SR micro-CT is also capable of generating edge-enhancing contrast known as 'phase contrast' (Betz et al., 2007, Meuli et al., 2004, Rustichelli et al., 2004), which has been shown to improve visualization of structures within mineralized tissues (Tafforeau and Smith, 2008). Incorporating the use of higher energies and phase contrast SR micro-CT should be able to reduce the radiation dose to a point where it is a viable technique for tracking remodeling events within rat cortical bone without being harmful to the rat. To date, in vivo SR micro-CT studies have focused on trabecular bone and have recorded doses of 5 grays (Gy) (Kinney et al., 1995, Matsumoto et al.). Studies have found that a single dose of 5 Gy impairs bone regeneration in rats, but a dose of 2.5 Gy has no measureable clinical effects (Jacobsson et al., 1985). To add some perspective, the average scan in a desktop in vivo micro-CT results in a dose somewhere between 300 and 400 mGy (milligrays), which has no detectable effect on bone architecture (Brouwers et al., 2007, Klinck and Boyd, 2006). In that sense, in vivo SR micro-CT still needs to be optimized in order to attain the resolutions necessary to track remodeling events within rat cortical bone while subjecting the rat to the smallest radiation dose possible.

With respect to the specimens used in this thesis, further investigation into how immobilization in Chapter 2 and the increased calcium demands in Chapter 3 affected osteocyte lacunae may be interesting. SR micro-CT has been shown to be capable of quantifying lacunar morphology (Schneider et al., 2007) and the use of phase contrast should enhance the visualization of the lacunae (Andrews et al., Power et al., 2001). One of the possible reasons for a lower remodeling rate in rats is that due to their size they may be able to fulfill their calcium requirements through the process of osteocytic osteolysis instead of remodeling. Osteocytic osteolysis is a process whereby osteocytes resorb bone within their localized lacunae (Belanger, 1969, Heller-Steinberg, 1951, Heuck, 1970, Krempien et al., 1973, Salomon and Volpin, 1970, Shea et al., 1968). One way to test this would be to measure lacunar volume and density in the bones from the experiment described in Chapter 3. If osteocytic osteolysis is capable of providing enough calcium to meet the rats requirements what would it mean in terms of bone adaptation in rats since load related stimuli play an important role in the health of the skeleton which dynamically adapts to the demands placed upon it? While gross morphological (Bennell et al., 2002, Howell, 1917, Rubin, 1984, Turner and Bell, 1986) and even tissue-level (Britz et al., 2010, Britz et al., 2009, Cooper et al., 2006, Cooper et al., 2007b, Cooper et al., 2003, Currey, 1988, Hert et al., 1994, Jee and Yao, 2001, Martin and Ishida, 1989, Petrtyl et al., 1996, Skedros et al., 1994a, Skedros et al., 1994b, Skedros et al., 1997, Yeni et al., 1997) adaptation have been the subject of much research, relatively little is known regarding cellular-level changes in morphology associated with loading. While the size, shape and density of lacunae have been proposed to reflect loading conditions, this link has yet to be definitely tested. Using SR micro-CT to look at

these measures in the specimens employed in Chapter 2 could shed some light on this area.

5.4 Conclusion

This thesis has set the ground work for developing a small animal model for looking at the 3D implications of loading on bone microarchitecture. I have demonstrated that vascular canals within rat cortical bone can be visualized and quantified in 3D using micro-CT. While it was not possible to discern primary from secondary canals using micro-CT, canal orientation was measurable. Vascular canals within the cortex of a normally ambulating rat limb are oriented more longitudinally than those found within an immobilized (paralyzed) limb (9.9°) indicating loading to be a factor in determining canal orientation. It must be noted that not only was loading but also type/direction of loading was found to be important in dictating canal orientation.

I was unable to verify whether calcium restriction alone or coupled with pregnancy and lactation provided a greater increase in remodeling. The information gained from that study has allowed me design a better experiment to address the development of a more effective way to induce remodeling in rats. Once remodeling is induced to a significant level a study similar to that outlined in Chapter 3 can be conducted to look at the effects loading has on remodeling event orientation. The most important contribution of this thesis is the development of a method capable of imaging and measuring vascular canal orientation within a small animal such as the rat. The full development of this animal model will allow researchers to address the hypotheses

concerning bone's ability to adapt to mechanical stimuli, ultimately leading to a better understanding of how loading affects cortical bone microarchitecture.

LIST OF REFERENCES

Altman DG, Bland JM (1983) Measurement in medicine: the analysis of method comparison studies. *Statistician,* **32,** 307-317.

Andrews JC, Almeida E, van der Meulen MC, et al. Nanoscale X-ray microscopic imaging of mammalian mineralized tissue. *Microsc Microanal,* **16,** 327-36.

Antonov SG (1980) [Effect of daily and intermittent dynamic loading on appositional growth and vascularization of the femoral diaphysis of rats]. *Arkh Anat Gistol Embriol,* **78,** 19-24.

Baca V, Kachlik D, Horak Z, Stingl J (2007) The course of osteons in the compact bone of thehuman proximal femur with clinical and biomechanical significance. *Surg Radiol Anat,* **29,** 201-207.

Bagi CM, Mecham M, Weiss J, Miller SC (1993) Comparative morphometric changes in rat cortical bone following ovariectomy and/or immobilization. *Bone,* **14,** 877-83.

Bakker AD, Joldersma M, Klein-Nulend J, Burger EH (2003) Interactive effects of PTH and mechanical stress on nitric oxide and PGE2 production by primary mouse osteoblastic cells. *Am J Physiol Endocrinol Metab,* **285,** E608-13.

Bakker AD, Soejima K, Klein-Nulend J, Burger EH (2001) The production of nitric oxide and prostaglandin E(2) by primary bone cells is shear stress dependent. *J Biomech,* **34,** 671-7.

Barbier A, Martel C, de Vernejoul MC, et al. (1999) The visualization and evaluation of bone architecture in the rat using three-dimensional X-ray microcomputed tomography. *J Bone Miner Metab,* **17,** 37-44.

Baron R (2003) Primer on the Metabolic Bone Diseases and Disorders of Mineral Metabolism. (ed Favus MJ), pp. 1-8.

Barou O, Mekraldi S, Vico L, Boivin G, Alexandre C, Lafage-Proust MH (2002a) Relationships between trabecular bone remodeling and bone vascularization: a quantitative study. *Bone,* **30,** 604-12.

Barou O, Valentin D, Vico L, et al. (2002b) High-resolution three-dimensional micro-computed tomography detects bone loss and changes in trabecular architecture early: comparison with DEXA and bone histomorphometry in a rat model of disuse osteoporosis. *Invest Radiol,* **37,** 40-6.

Barth RW, Williams JL, Kaplan FS (1992) Osteon morphometry in females with femoral neck fractures. *Clin Orthop Relat Res***,** 178-86.

Basillais A, Bensamoun S, Chappard C, et al. (2007) Three-dimensional characterization of cortical bone microstructure by microcomputed tomography: validation with ultrasonic and microscopic measurements. *J Orthop Sci,* **12,** 141-8.

Bawden JW, McIver FT (1964) Distribution of Ca-45 during Pregnancy under Conditions of Calcium Deficiency in Rats. *J Dent Res,* **43,** 563-7.

Belanger LF (1969) Osteocytic osteolysis. *Calcif Tissue Res,* **4,** 1-12.

Bell RR, Tzeng DY, Draper HH (1980) Long-term effects of calcium, phosphorus and forced exercise on the bones of mature mice. *J Nutr,* **110,** 1161-8.

Bennell KL, Khan KM, Warmington S, et al. (2002) Age does not influence the bone response to treadmill exercise in female rats. *Med Sci Sports Exerc,* **34,** 1958-65.

Bernhardt R, Scharnweber D, Muller B, et al. (2004) Comparison of microfocus- and synchrotron X-ray tomography for the analysis of osteointegration around Ti6Al4V implants. *Eur Cell Mater,* **7,** 42-51; discussion 51.

Betz O, Wegst U, Weide D, et al. (2007) Imaging applications of synchrotron X-ray phase-contrast microtomography in biological morphology and biomaterials science. I. General aspects of the technique and its advantages in the analysis of millimetre-sized arthropod structure. *J Microsc,* **227,** 51-71.

Borah B, Dufresne T, Nurre J, et al. (2009) Risedronate Reduces Intracortical Porosity in Women with Osteoporosis. *J Bone Miner Res*.

Bousson V, Peyrin F, Bergot C, Hausard M, Sautet A, Laredo JD (2004) Cortical bone in the human femoral neck: three-dimensional appearance and porosity using synchrotron radiation. *J Bone Miner Res,* **19,** 794-801.

Boyd SK, Moser S, Kuhn M, et al. (2006) Evaluation of three-dimensional image registration methodologies for in vivo micro-computed tomography. *Ann Biomed Eng,* **34,** 1587-99.

Britz HM, Jokihaara J, Leppanen OV, Jarvinen T, Cooper DM (2010) 3D visualization and quantification of rat cortical bone porosity using a desktop micro-CT system: a case study in the tibia. *J Microsc,* **240,** 32-7.

Britz HM, Thomas CD, Clement JG, Cooper DM (2009) The relation of femoral osteon geometry to age, sex, height and weight. *Bone,* **45,** 77-83.

Brommage R, DeLuca HF (1985) Regulation of bone mineral loss during lactation. *Am J Physiol,* **248,** E182-7.

Brouwers JE, van Rietbergen B, Huiskes R (2007) No effects of in vivo micro-CT radiation on structural parameters and bone marrow cells in proximal tibia of wistar rats detected after eight weekly scans. *J Orthop Res,* **25,** 1325-32.

Burger EH, Klein-Nulend J, Smit TH (2003) Strain-derived canalicular fluid flow regulates osteoclast activity in a remodelling osteon--a proposal. *J Biomech,* **36,** 1453-9.

Campbell GM, Ominsky MS, Boyd SK Bone quality is partially recovered after the discontinuation of RANKL administration in rats by increased bone mass on existing trabeculae: an in vivo micro-CT study. *Osteoporos Int,* **22,** 931-42.

Carter DR, Hayes WC, Schurman DJ (1976) Fatigue life of compact bone--II. Effects of microstructure and density. *J Biomech,* **9,** 211-8.

Castanet J, Grandin A, Abourachid A, de Ricqles A (1996) [Expression of growth dynamic in the structure of periosteal bone in Anas platyrhynchos]. *C R Acad Sci III,* **319,** 301-8.

Castanet J, Rogers KC, Cubo J, Boisard JJ (2000) Periosteal bone growth rates in extant ratites (ostriche and emu). Implications for assessing growth in dinosaurs. *C R Acad Sci III,* **323,** 543-50.

Chen H, Zhou X, Shoumura S, Emura S, Bunai Y (2009) Age- and gender-dependent changes in three-dimensional microstructure of cortical and trabecular bone at the human femoral neck. *Osteoporos Int*.

Cohen I, Bogin E, Chechick A, Rzetelny V (1999) The effect of single hind-limb immobilization on the contralateral limb in the rat: a morphometric and biochemical study. *Am J Orthop (Belle Mead NJ),* **28,** 706-8.

Cohen J, Harris WH (1958) The three-dimensional anatomy of haversian systems. *J Bone Joint Surg Am,* **40-A,** 419-34.

Cooper D, Turinsky A, Sensen C, Hallgrimsson B (2007a) Effect of voxel size on 3D micro-CT analysis of cortical bone porosity. *Calcif Tissue Int,* **80,** 211-9.

Cooper DM, Ahamed Y, Macdonald HM, McKay HA (2008) Characterising cortical density in the mid-tibia: intra-individual variation in adolescent girls and boys. *Br J Sports Med,* **42,** 690-5.

Cooper DM, Matyas JR, Katzenberg MA, Hallgrimsson B (2004) Comparison of microcomputed tomographic and microradiographic measurements of cortical bone porosity. *Calcif Tissue Int,* **74,** 437-47.

Cooper DM, Thomas CD, Clement JG, Hallgrimsson B (2006) Three-dimensional microcomputed tomography imaging of basic multicellular unit-related resorption spaces in human cortical bone. *Anat Rec A Discov Mol Cell Evol Biol,* **288,** 806-16.

Cooper DM, Thomas CD, Clement JG, Turinsky AL, Sensen CW, Hallgrimsson B (2007b) Age-dependent change in the 3D structure of cortical porosity at the human femoral midshaft. *Bone,* **40,** 957-65.

Cooper DM, Turinsky AL, Sensen CW, Hallgrimsson B (2003) Quantitative 3D analysis of the canal network in cortical bone by micro-computed tomography. *Anat Rec B New Anat,* **274,** 169-79.

Cowin SC, Moss ML (2001) Mechanosensory mechanisms in bone. In *Bone biomechanics handbook* (ed Cowin SC), pp. 29-1 - 29-17 Boca Raton: CRC Press.

Cowin SC, Weinbaum S, Zeng Y (1995) A case for bone canaliculi as the anatomical site of strain generated potentials. *J Biomech,* **28,** 1281-97.

Currey JD (1988) The effect of porosity and mineral content on the Young's modulus of elasticity of compact bone. *J Biomech,* **21,** 131-9.

Currey JD, Hughes SM (1973) The effects of pregnancy and lactation on some mechanical properties of the femora of the rat. *Calcif Tissue Res,* **11,** 112-23.

Davidson RM, Lingenbrink PA, Norton LA (1996) Continuous mechanical loading alters properties of mechanosensitive channels in G292 osteoblastic cells. *Calcif Tissue Int,* **59,** 500-4.

de Margerie E (2002) Laminar bone as an adaptation to torsional loads in flapping flight. *J Anat,* **201,** 521-6.

de Margerie E, Cubo J, Castanet J (2002) Bone typology and growth rate: testing and quantifying 'Amprino's rule' in the mallard (Anas platyrhynchos). *C R Biol,* **325,** 221-30.

de Margerie E, Sanchez S, Cubo J, Castanet J (2005) Torsional resistance as a principal component of the structural design of long bones: comparative multivariate evidence in birds. *Anat Rec A Discov Mol Cell Evol Biol,* **282,** 49-66.

de Souza RL, Pitsillides AA, Lanyon LE, Skerry TM, Chenu C (2005) Sympathetic nervous system does not mediate the load-induced cortical new bone formation. *J Bone Miner Res,* **20,** 2159-68.

de Winter FR, Steendijk R (1975) The effect of a low-calcium diet in lactating rats; observations on the rapid development and repair of osteoporosis. *Calcif Tissue Res,* **17,** 303-16.

Dellon ES, Dellon AL (1991) Functional assessment of neurologic impairment: track analysis in diabetic and compression neuropathies. *Plast Reconstr Surg,* **88,** 686-94.

Dilmanian FA (1992) Computed tomography with monochromatic x rays. *Am J Physiol Imaging,* **7,** 175-93.

Dodd JS, Raleigh JA, Gross TS (1999) Osteocyte hypoxia: a novel mechanotransduction pathway. *Am J Physiol,* **277,** C598-602.

Ellinger GM, Duckworth J, Dalgarno AC, Quenouille MH (1952) Skeletal changes during pregnancy and lactation in the rat: effect of different levels of dietary calcium. *Br J Nutr,* **6,** 235-53.

Evans FG, Bang S (1967) Differences and Relationships between Physical Properties and Microscopic Structure of Human Femoral Tibial and Fibular Cortical Bone. *American Journal of Anatomy,* **120,** 79-&.

Evans FG, Vincentelli R (1974) Relations of the compressive properties of human cortical bone to histological structure and calcification. *J Biomech,* **7,** 1-10.

Fajardo RJ, Ryan TM, Kappelman J (2002) Assessing the accuracy of high-resolution X-ray computed tomography of primate trabecular bone by comparisons with histological sections. *Am J Phys Anthropol,* **118,** 1-10.

Feldkamp LA, Goldstein SA, Parfitt AM, Jesion G, Kleerekoper M (1989) The direct examination of three-dimensional bone architecture in vitro by computed tomography. *J Bone Miner Res,* **4,** 3-11.

Ford NL, Thornton MM, Holdsworth DW (2003) Fundamental image quality limits for microcomputed tomography in small animals. *Med Phys,* **30,** 2869-77.

Frost HM (1958) Preparation of thin undecalcified bone sections by rapid manual method. *Stain Technol,* **33,** 273-7.

Gartner LP, Hiatt JL (1997) *Color Textbook of Histology*.

Grodzins L (1983) Critical Absorption Tomography of Small Samples - Proposed Applications of Synchrotron Radiation to Computerized-Tomography .2. *Nuclear Instruments & Methods in Physics Research,* **206,** 547-552.

Guggino SE, Lajeunesse D, Wagner JA, Snyder SH (1989) Bone remodeling signaled by a dihydropyridine- and phenylalkylamine-sensitive calcium channel. *Proc Natl Acad Sci U S A,* **86,** 2957-60.

Heller-Steinberg M (1951) Ground substance, bone salts, and cellular activity in bone formation and destruction. *Am J Anat,* **89,** 347-79.

Hert J, Fiala P, Petrtyl M (1994) Osteon orientation of the diaphysis of the long bones in man. *Bone,* **15,** 269-77.

Hert J, Sklenska A, Liskova M (1971) Reaction of bone to mechanical stimuli. 5. Effect of intermittent stress on the rabbit tibia after resection of the peripheral nerves. *Folia Morphol (Praha),* **19,** 378-87.

Heuck F (1970) Comparative investigations of the function of osteocytes in bone resorption. *Calcif Tissue Res***,** Suppl:148-9.

Hildebrand T, Laib A, Muller R, Dequeker J, Ruegsegger P (1999) Direct three-dimensional morphometric analysis of human cancellous bone: microstructural data from spine, femur, iliac crest, and calcaneus. *J Bone Miner Res,* **14,** 1167-74.

Hildebrand T, Ruegsegger P (1997) A new method for the model-independent assessment of thickness in three-dimensional images. *Journal of Microscopy-Oxford,* **185,** 67-75.

Hounsfield GN (1973) Computerized transverse axial scanning (tomography). 1. Description of system. *Br J Radiol,* **46,** 1016-22.

Howell JA (1917) An experimental study of the effect of stress and strain on bone development. *Anatomical Record,* **13,** 233-252.

Ito M, Nakamura T, Matsumoto T, Tsurusaki K, Hayashi K (1998) Analysis of trabecular microarchitecture of human iliac bone using microcomputed tomography in patients with hip arthrosis with or without vertebral fracture. *Bone,* **23,** 163-9.

Jacobsson M, Jonsson A, Albrektsson T, Turesson I (1985) Alterations in bone regenerative capacity after low level gamma irradiation. A quantitative study. *Scand J Plast Reconstr Surg,* **19,** 231-6.

Järvinen TL, Kannus P, Pajamaki I, et al. (2003a) Estrogen deposits extra mineral into bones of female rats in puberty, but simultaneously seems to suppress the responsiveness of female skeleton to mechanical loading. *Bone,* **32,** 642-51.

Järvinen TL, Pajamaki I, Sievanen H, et al. (2003b) Femoral neck response to exercise and subsequent deconditioning in young and adult rats. *J Bone Miner Res,* **18,** 1292-9.

Jee WS, Yao W (2001) Overview: animal models of osteopenia and osteoporosis. *J Musculoskelet Neuronal Interact,* **1,** 193-207.

Jiang Y, Zhao J, White DL, Genant HK (2000) Micro CT and Micro MR imaging of 3D architecture of animal skeleton. *J Musculoskelet Neuronal Interact,* **1,** 45-51.

Jones AC, Arns CH, Hutmacher DW, Milthorpe BK, Sheppard AP, Knackstedt MA (2009) The correlation of pore morphology, interconnectivity and physical properties of 3D ceramic scaffolds with bone ingrowth. *Biomaterials,* **30,** 1440-51.

Jones AC, Milthorpe B, Averdunk H, et al. (2004) Analysis of 3D bone ingrowth into polymer scaffolds via micro-computed tomography imaging. *Biomaterials,* **25,** 4947-54.

Jowsey J (1966) Studies of Haversian Systems in Man and Some Animals. *Journal of Anatomy,* **100,** 857-&.

Kingery WS, Offley SC, Guo TZ, Davies MF, Clark JD, Jacobs CR (2003) A substance P receptor (NK1) antagonist enhances the widespread osteoporotic effects of sciatic nerve section. *Bone,* **33,** 927-36.

Kinney JH, Lane NE, Haupt DL (1995) In vivo, three-dimensional microscopy of trabecular bone. *J Bone Miner Res,* **10,** 264-70.

Kleerekoper M, Villanueva AR, Stanciu J, Rao DS, Parfitt AM (1985) The role of three-dimensional trabecular microstructure in the pathogenesis of vertebral compression fractures. *Calcif Tissue Int,* **37,** 594-7.

Klein-Nulend J, Sterck JG, Semeins CM, et al. (2002) Donor age and mechanosensitivity of human bone cells. *Osteoporos Int,* **13,** 137-46.

Klinck RJ, Boyd SK (2006) The effects of radiation on ovariectomized mice as a function of genetic strain by in vivo micro-computed tomography. *Journal of Bone and Mineral Research,* **21,** S230-S230.

Koch J (1917) The laws of bone architecture. *Am J Anat,* **21,** 177-298.

Komarkova A, Zahor Z, Czabanova V (1967) The effect of lactaion on the composition of long bones in rats. . *J. Lab Clin Med,* **69,** 102-109.

Krempien B, Geiger G, Ritz E, Buttner S (1973) Osteocytes in chronic uremia. Differential count of osteocytes in human femoral bone. *Virchows Arch A Pathol Pathol Anat,* **360,** 1-9.

Kuhn JL, Goldstein SA, Feldkamp LA, Goulet RW, Jesion G (1990) Evaluation of a microcomputed tomography system to study trabecular bone structure. *J Orthop Res,* **8,** 833-42.

Lanyon LE, Baggott DG (1976) Mechanical function as an influence on the structure and form of bone. *J Bone Joint Surg Br,* **58-B,** 436-43.

Lanyon LE, Bourn S (1979) The influence of mechanical function on the development and remodeling of the tibia. An experimental study in sheep. *J Bone Joint Surg Am,* **61,** 263-73.

Leopold SS, Boskey AL, Doty SB, Gertner JM, Peterson MG, Torzilli PA (1995) Diminished material properties and altered bone structure in rat femora during pregnancy. *J Orthop Res,* **13,** 41-9.

Leppänen OV, Sievanen H, Jokihaara J, et al. (2010) The effects of loading and estrogen on rat bone growth. *J Appl Physiol,* **108,** 1737-44.

Leppänen OV, Sievanen H, Jokihaara J, Pajamaki I, Kannus P, Jarvinen TL (2008) Pathogenesis of age-related osteoporosis: impaired mechano-responsiveness of bone is not the culprit. *PLoS One,* **3,** e2540.

Li KC, Zernicke RF, Barnard RJ, Li AF (1991) Differential response of rat limb bones to strenuous exercise. *J Appl Physiol,* **70,** 554-60.

Lozupone E, Favia A (1988) Distribution of resorption processes in the compacta and spongiosa of bones from lactating rats fed a low-calcium diet. *Bone,* **9,** 215-24.

Malushte TS, Kerns JM, Huang CC, Shott S, Safanda J, Gonzalez M (2004) Assessment of recovery following a novel partial nerve lesion in a rat model. *Muscle Nerve,* **30,** 609-17.

Marotti G (1996) The structure of bone tissues and the cellular control of their deposition. *Ital J Anat Embryol,* **101,** 25-79.

Martin RB (2002) Is all cortical bone remodeling initiated by microdamage? *Bone,* **30,** 8-13.

Martin RB (2003) Fatigue damage, remodeling, and the minimization of skeletal weight. *J Theor Biol,* **220,** 271-6.

Martin RB, Ishida J (1989) The relative effects of collagen fiber orientation, porosity, density, and mineralization on bone strength. *J Biomech,* **22,** 419-26.

Matsumoto T, Nishikawa K, Tanaka M, Uesugi K In Vivo CT Quantification of Trabecular Bone Dynamics in Mice after Sciatic Neurectomy Using Monochromatic Synchrotron Radiation. *Calcif Tissue Int*.

Matsumoto T, Yoshino M, Asano T, Uesugi K, Todoh M, Tanaka M (2006) Monochromatic synchrotron radiation muCT reveals disuse-mediated canal network rarefaction in cortical bone of growing rat tibiae. *J Appl Physiol,* **100,** 274-80.

Matsumoto T, Yoshino M, Uesugi K, Tanaka M (2007) Biphasic change and disuse-mediated regression of canal network structure in cortical bone of growing rats. *Bone,* **41,** 239-46.

McCalden RW, McGeough JA, Barker MB, Court-Brown CM (1993) Age-related changes in the tensile properties of cortical bone. The relative importance of changes in porosity, mineralization, and microstructure. *J Bone Joint Surg Am,* **75,** 1193-205.

McDonald R, Hegenauer J, Saltman P (1986) Age-related differences in the bone mineralization pattern of rats following exercise. *J Gerontol,* **41,** 445-52.

Meuli R, Hwu Y, Je JH, Margaritondo G (2004) Synchrotron radiation in radiology: radiology techniques based on synchrotron sources. *Eur Radiol,* **14,** 1550-60.

Mickel W, Munster S, Jawerth LM, et al. (2008) Robust pore size analysis of filamentous networks from three-dimensional confocal microscopy. *Biophys J,* **95,** 6072-80.

Miller SC, Bowman BM (2004) Rapid improvements in cortical bone dynamics and structure after lactation in established breeder rats. *Anat Rec A Discov Mol Cell Evol Biol,* **276,** 143-9.

Miller SC, Shupe JG, Redd EH, Miller MA, Omura TH (1986) Changes in bone mineral and bone formation rates during pregnancy and lactation in rats. *Bone,* **7,** 283-7.

Mohsin S, Taylor D, Lee TC (2002) Three-dimensional reconstruction of Haversian systems in ovine compact bone. *Eur J Morphol,* **40,** 309-15.

Muller R, Koller B, Hildebrand T, Laib A, Gianolini S, Ruegsegger P (1996) Resolution dependency of microstructural properties of cancellous bone based on three-dimensional mu-tomography. *Technol Health Care,* **4,** 113-9.

Muller R, Van Campenhout H, Van Damme B, et al. (1998) Morphometric analysis of human bone biopsies: a quantitative structural comparison of histological sections and micro-computed tomography. *Bone,* **23,** 59-66.

Mullins LP, McGarry JP, Bruzzi MS, McHugh PE (2007) Micromechanical modelling of cortical bone. *Comput Methods Biomech Biomed Engin,* **10,** 159-69.

Nango N, Kubota S, Takeda Y, Yashiro W, Momose A, Matsuo K (2010) Structural Basis for Bone Resorption within the Cortical Bone. In *American Society of Bone and Mineral Research*). Toronto, Canada.

Notomi T, Lee SJ, Okimoto N, et al. (2000) Effects of resistance exercise training on mass, strength, and turnover of bone in growing rats. *Eur J Appl Physiol,* **82,** 268-74.

Pajamaki I, Kannus P, Vuohelainen T, et al. (2003) The bone gain induced by exercise in puberty is not preserved through a virtually life-long deconditioning: a randomized controlled experimental study in male rats. *J Bone Miner Res,* **18,** 544-52.

Parfitt AM (2002) Targeted and nontargeted bone remodeling: relationship to basic multicellular unit origination and progression. *Bone,* **30,** 5-7.

Parfitt AM, Mathews CH, Villanueva AR, Kleerekoper M, Frame B, Rao DS (1983) Relationships between surface, volume, and thickness of iliac trabecular bone in aging and in osteoporosis. Implications for the microanatomic and cellular mechanisms of bone loss. *J Clin Invest,* **72,** 1396-409.

Parker AW (1977) Changes in Vascularity of Femoral Cortex of Rat Following Exercise. *Journal of Anatomy,* **124,** 525-525.

Pazzaglia UE, Bonaspetti G, Ranchetti F, Bettinsoli P (2008) A model of the intracortical vascular system of long bones and of its organization: an experimental study in rabbit femur and tibia. *J Anat,* **213,** 183-93.

Pazzaglia UE, Zarattini G, Giacomini D, Rodella L, Menti AM, Feltrin G (2010) Morphometric analysis of the canal system of cortical bone: An experimental study in the rabbit femur carried out with standard histology and micro-CT. *Anat Histol Embryol,* **39,** 17-26.

Pearson OM, Lieberman DE (2004) The aging of Wolff's "law": ontogeny and responses to mechanical loading in cortical bone. *Am J Phys Anthropol,* **Suppl 39,** 63-99.

Peterman MM, Hamel AJ, Cavanagh PR, Piazza SJ, Sharkey NA (2001) In vitro modeling of human tibial strains during exercise in micro-gravity. *J Biomech,* **34,** 693-8.

Petrtyl M, Hert J, Fiala P (1996) Spatial organization of the haversian bone in man. *J Biomech,* **29,** 161-9.

Peyrin F (2009) Investigation of bone with synchrotron radiation imaging: from micro to nano. *Osteoporos Int,* **20,** 1057-63.

Peyrin F, Salome M, Nuzzo S, Cloetens P, Laval-Jeantet AM, Baruchel J (2000) Perspectives in three-dimensional analysis of bone samples using synchrotron radiation microtomography. *Cell Mol Biol (Noisy-le-grand),* **46,** 1089-102.

Power J, Noble BS, Loveridge N, Bell KL, Rushton N, Reeve J (2001) Osteocyte lacunar occupancy in the femoral neck cortex: an association with cortical remodeling in hip fracture cases and controls. *Calcif Tissue Int,* **69,** 13-9.

Raab DM, Crenshaw TD, Kimmel DB, Smith EL (1991) A histomorphometric study of cortical bone activity during increased weight-bearing exercise. *J Bone Miner Res,* **6,** 741-9.

Rasmussen P (1977a) Calcium deficiency, pregnancy, and lactation in rats. Microscopic and microradiographic observations on bones. *Calcif Tissue Res,* **23,** 95-102.

Rasmussen P (1977b) Calcium deficiency, pregnancy, and lactation in rats. Some effects on blood chemistry and the skeleton. *Calcif Tissue Res,* **23,** 87-94.

Ream JL, Hull DL, Scott JN, Pendergrass PB (1983) Fluoride ingestion during multiple pregnancies and lactations: microscopic observations on bone of the rat. *Virchows Arch B Cell Pathol Incl Mol Pathol,* **44,** 35-44.

Recker RR (1993) Architecture and vertebral fracture. *Calcif Tissue Int,* **53 Suppl 1,** S139-42.

Renders GAP, Mulder L, van Ruijven LJ, van Eijden TMGJ (2007) Porosity of human mandibular condylar bone. *Journal of Anatomy,* **210,** 239-248.

Robling AG, Bellido T, Turner CH (2006) Mechanical stimulation in vivo reduces osteocyte expression of sclerostin. *J Musculoskelet Neuronal Interact,* **6,** 354.

Rubin CT (1984) Skeletal strain and the functional significance of bone architecture. *Calcif Tissue Int,* **36 Suppl 1,** S11-8.

Rustichelli F, Romanzetti S, Dubini B, et al. (2004) Phase-contrast microtomography of thin biomaterials. *J Mater Sci Mater Med,* **15,** 1053-7.

Ruth EB (1953) Bone studies. II. An experimental study of the Haversian-type vascular channels. *Am J Anat,* **93,** 429-55.

Salomon CD, Volpin G (1970) Fine structure of bone resorption in experimental osteoporosis caused by calcium deficient diet in rats. An electron microscopic study of compact bone. *Calcif Tissue Res***,** Suppl:80-2.

Schaffler MB, Burr DB (1988) Stiffness of compact bone: effects of porosity and density. *J Biomech,* **21,** 13-6.

Schneider P, Krucker T, Meyer E, et al. (2009) Simultaneous 3D visualization and quantification of murine bone and bone vasculature using micro-computed tomography and vascular replica. *Microsc Res Tech,* **72,** 690-701.

Schneider P, Stauber M, Voide R, Stampanoni M, Donahue LR, Muller R (2007) Ultrastructural properties in cortical bone vary greatly in two inbred strains of mice as assessed by synchrotron light based micro- and nano-CT. *J Bone Miner Res,* **22,** 1557-70.

Seeman E (2004) The growth and age-related origins of bone fragility in men. *Calcif Tissue Int,* **75,** 100-9.

Sevostianov I, Kachanov M (2000) Impact of the porous microstructure on the overall elastic properties of the osteonal cortical bone. *J Biomech,* **33,** 881-8.

Shea JF, Yeager VL, Taylor JJ (1968) Bone resorption by osteocytes. *Proc Soc Exp Biol Med,* **129,** 41-3.

Skedros JG, Bloebaum RD, Mason MW, Bramble DM (1994a) Analysis of a tension/compression skeletal system: possible strain-specific differences in the hierarchical organization of bone. *Anat Rec,* **239,** 396-404.

Skedros JG, Mason MW, Bloebaum RD (1994b) Differences in osteonal micromorphology between tensile and compressive cortices of a bending skeletal system: indications of potential strain-specific differences in bone microstructure. *Anat Rec,* **239,** 405-13.

Skedros JG, Su SC, Bloebaum RD (1997) Biomechanical implications of mineral content and microstructural variations in cortical bone of horse, elk, and sheep calcanei. *Anat Rec,* **249,** 297-316.

Smit TH, Burger EH (2000) Is BMU-coupling a strain-regulated phenomenon? A finite element analysis. *J Bone Miner Res,* **15,** 301-7.

Smit TH, Burger EH, Huyghe JM (2002) A case for strain-induced fluid flow as a regulator of BMU-coupling and osteonal alignment. *J Bone Miner Res,* **17,** 2021-9.

Sonoda N, Chosa E, Totoribe K, Tajima N (2003) Biomechanical analysis for stress fractures of the anterior middle third of the tibia in athletes: nonlinear analysis using a three-dimensional finite element method. *J Orthop Sci,* **8,** 505-13.

Spray CM (1950) A study of some aspects of reproduction by means of chemical analysis. *Br J Nutr,* **4,** 354-60.

Steinberg ME, Trueta J (1981) Effects of activity on bone growth and development in the rat. *Clin Orthop Relat Res***,** 52-60.

Stout SD, Brunsden BS, Hildebolt CF, Commean PK, Smith KE, Tappen NC (1999) Computer-assisted 3D reconstruction of serial sections of cortical bone to determine the 3D structure of osteons. *Calcif Tissue Int,* **65,** 280-4.

Swartz SM, Bennett MB, Carrier DR (1992) Wing bone stresses in free flying bats and the evolution of skeletal design for flight. *Nature,* **359,** 726-9.

Tafforeau P, Smith TM (2008) Nondestructive imaging of hominoid dental microstructure using phase contrast X-ray synchrotron microtomography. *J Hum Evol,* **54,** 272-8.

Tappen NC (1977) Three-dimensional studies on resorption spaces and developing osteons. *Am J Anat,* **149,** 301-17.

Teitelbaum SL (2000) Bone resorption by osteoclasts. *Science,* **289,** 1504-8.

Tomes J, de Morgan C (1853) Observations on the Structure and Development of Bone. *Philos Trans R Soc Lond B Biol Sci,* **143,** 109-139.

Tondevold E (1983) Haemodynamics of long bones. An experimental study on dogs. *Acta Orthop Scand Suppl,* **205,** 9-48.

Tondevold E, Bulow J (1983) Bone blood flow in conscious dogs at rest and during exercise. *Acta Orthop Scand,* **54,** 53-7.

Turner RT, Bell NH (1986) The effects of immobilization on bone histomorphometry in rats. *J Bone Miner Res,* **1,** 399-407.

Uchiyama T, Tanizawa T, Muramatsu H, Endo N, Takahashi HE, Hara T (1997) A morphometric comparison of trabecular structure of human ilium between microcomputed tomography and conventional histomorphometry. *Calcif Tissue Int,* **61,** 493-8.

Uhthoff HK, Jaworski ZF (1978) Bone loss in response to long-term immobilisation. *J Bone Joint Surg Br,* **60-B,** 420-9.

Vajda EG, Bowman BM, Miller SC (2001) Cancellous and cortical bone mechanical properties and tissue dynamics during pregnancy, lactation, and postlactation in the rat. *Biol Reprod,* **65,** 689-95.

van Oers RF, Ruimerman R, Tanck E, Hilbers PA, Huiskes R (2008a) A unified theory for osteonal and hemi-osteonal remodeling. *Bone,* **42,** 250-9.

van Oers RF, Ruimerman R, van Rietbergen B, Hilbers PA, Huiskes R (2008b) Relating osteon diameter to strain. *Bone,* **43,** 476-82.

Verhaeghe J, Thomsen JS, van Bree R, van Herck E, Bouillon R, Mosekilde L (2000) Effects of exercise and disuse on bone remodeling, bone mass, and

biomechanical competence in spontaneously diabetic female rats. *Bone,* **27,** 249-56.

Vincentelli R, Grigorov M (1985) The effect of Haversian remodeling on the tensile properties of human cortical bone. *J Biomech,* **18,** 201-7.

Voide R, Schneider P, Stauber M, et al. (2009) Time-lapsed assessment of microcrack initiation and propagation in murine cortical bone at submicrometer resolution. *Bone,* **45,** 164-73.

Waarsing JH, Day JS, van der Linden JC, et al. (2004) Detecting and tracking local changes in the tibiae of individual rats: a novel method to analyse longitudinal in vivo micro-CT data. *Bone,* **34,** 163-9.

Wachter NJ, Augat P, Krischak GD, Mentzel M, Kinzl L, Claes L (2001) Prediction of cortical bone porosity in vitro by microcomputed tomography. *Calcif Tissue Int,* **68,** 38-42.

Wolff J (1892) *Das Gesetz der Transformation der Knochen,* Springer Verlag, Berlin, Germany.

Woo SL, Kuei SC, Amiel D, et al. (1981) The effect of prolonged physical training on the properties of long bone: a study of Wolff's Law. *J Bone Joint Surg Am,* **63,** 780-7.

Yeni YN, Brown CU, Wang Z, Norman TL (1997) The influence of bone morphology on fracture toughness of the human femur and tibia. *Bone,* **21,** 453-9.

Young DR, Niklowitz WJ, Brown RJ, Jee WS (1986) Immobilization-associated osteoporosis in primates. *Bone,* **7,** 109-17.

Zeman HD, Siddons DP (1990) Contrast Agent Choice for Intravenous Coronary Angiography. *Nuclear Instruments & Methods in Physics Research Section a-Accelerators Spectrometers Detectors and Associated Equipment,* **291,** 67-73.

APPENDIX A

ETHICS APPROVAL

UNIVERSITY OF SASKATCHEWAN

Animal Research Ethics Board (AREB)

Certificate of Approval
Protocol Modification

PRINCIPAL INVESTIGATOR	DEPARTMENT/ORGANIZATION	ANIMAL USE PROTOCOL #
Dr. David Cooper	Anatomy & Cell Biology	20080050

TITLE
Micro-CT imaging analysis of 3D microstructural changes in rat cortical bone induced by unloading

APPROVAL DATE:	APPROVAL OF:	EXPIRY DATE:
November 8, 2010	Change experimetnal design or procedures	November 1, 2011

Full Board Meeting ☐ AREB Subcommittee ☐ AREB Chair and University Veterinarian ☐ AREB Chair ☒

CERTIFICATION
The University of Saskatchewan Animal Research Ethics Board reviewed the above-named research project. The proposal was found to be acceptable on ethical grounds. The principal investigator has the responsibility for any other administrative or regulatory approvals that may pertain to this research project, and for ensuring that the authorized research is carried out according to the conditions outlined in the original protocol submitted for ethics review. This Certificate of Approval is valid for the above time period.

ONGOING REVIEW REQUIREMENTS
Research programs that extend beyond one year must receive annual review. For the annual renewal, an annual review form (and progress report) must be submitted to the AREB within one month of the current expiry date each year the study remains open, and upon study completion. Please refer to the Research Ethics Office website for further instructions.

PROTOCOL MODIFICATIONS
Any further modifications to this protocol must be approved by the UCACS AREB prior to implementation, using the AUP Modification Form.

Jane Alcorn, DVM, PhD, Chair
Animal Research Ethics Board
University of Saskatchewan

November 15, 2010
Date Issued

Please send all correspondence to:

Research Ethics Office
University of Saskatchewan
Box 5000 RPO University, 1607-110 Gymnasium Place
Saskatoon SK S7N 4J8
Telephone: (306) 966-4126 Fax: (306) 966-2069

UNIVERSITY OF SASKATCHEWAN

Animal Research Ethics Board (AREB)

Certificate of Approval

PRINCIPAL INVESTIGATOR
Dr. David Cooper

DEPARTMENT/ORGANIZATION
Anatomy & Cell Biology

ANIMAL USE PROTOCOL #
20100097

TITLE
Development of A Rat Model To Study The 3D Regulation of Cortical Bone Remodeling

SPONSORING AGENCIES
Natural Sciences Engineering Research Council (NSERC)

BIOSAFETY NUMBER
ANA-14

UNIFI FUND #
408013

APPROVAL DATE:
October 26, 2010

APPROVAL OF:
New Animal Use Protocol

EXPIRY DATE:
October 26, 2011

Full Board Meeting ☒ AREB Subcommittee ☐ AREB Chair and University Veterinarian ☐ AREB Chair ☐

CERTIFICATION
The University of Saskatchewan Animal Research Ethics Board reviewed the above-named research project. The proposal was found to be acceptable on ethical grounds. The principal investigator has the responsibility for any other administrative or regulatory approvals that may pertain to this research project, and for ensuring that the authorized research is carried out according to the conditions outlined in the original protocol submitted for ethics review. This Certificate of Approval is valid for the above time period.

PROTOCOL MODIFICATIONS
Any modifications to this protocol must be approved by the UCACS AREB Chair prior to implementation, using the AUP Modification Form.

ONGOING REVIEW REQUIREMENTS
Research programs that extend beyond one year must receive annual review. For the annual renewal, an annual review form (and progress report) must be submitted to the AREB within one month of the current expiry date each year the study remains open, and upon study completion. Please refer to the Research Ethics Office website for further instructions.

PLEASE NOTE THE FOLLOWING:
The AREB approves the use of six rats for your pilot study: 2 males; 2 females used on calcium restricted diet; and 2 females used for pregnancy and lactation on the calcium restricted diet (plus 24 pups).

A report detailing the results of your pilot study must be submitted to the AREB for review and approval before the AREB will issue a Certificate of Approval for the full study.

Jane Alcorn, DVM, PhD, Chair
Animal Research Ethics Board
University of Saskatchewan

October 26, 2010
Date Issued

Please send all correspondence to:

Research Ethics Office
University of Saskatchewan
Box 5000 RPO University, 1607-110 Gymnasium Place
Saskatoon SK S7N 4J8
Telephone: (306) 966-7928 Fax: (306) 966-2069 Email: ucacs.office@usask.ca

APPENDIX B

JOURNAL PUBLICATION PERMISSION

JOHN WILEY AND SONS LICENSE TERMS AND CONDITIONS

Aug 15, 2011

This is a License Agreement between Hayley M Britz ("You") and John Wiley and Sons ("John Wiley and Sons") provided by Copyright Clearance Center ("CCC"). The license consists of your order details, the terms and conditions provided by John Wiley and Sons, and the payment terms and conditions.

All payments must be made in full to CCC. For payment instructions, please see information listed at the bottom of this form.

License Number	2730360449724
License date	Aug 15, 2011
Licensed content publisher	John Wiley and Sons
Licensed content publication	Journal of Microscopy
Licensed content title	3D visualization and quantification of rat cortical bone porosity using a desktop micro-CT system: a case study in the tibia
Licensed content author	H.M. BRITZ,J. JOKIHAARA,O.V. LEPP□?NEN,T. J□?RVINEN,D.M.L. COOPER
Licensed content date	Oct 1, 2010
Start page	32
End page	37
Type of use	Dissertation/Thesis
Requestor type	Author of this Wiley article
Format	Electronic
Portion	Full article
Will you be translating?	No
Order reference number	
Total	0.00 USD

Terms and Conditions

TERMS AND CONDITIONS

This copyrighted material is owned by or exclusively licensed to John Wiley & Sons, Inc. or one of its group companies (each a "Wiley Company") or a society for whom a Wiley Company has exclusive publishing rights in relation to a particular journal (collectively WILEY"). By clicking "accept" in connection with completing this licensing transaction, you agree that the following terms and conditions apply to this transaction (along with the billing and payment terms and conditions established by the Copyright Clearance Center Inc., ("CCC's Billing and Payment terms and conditions"), at the time that you opened your Rightslink account (these are available at any time at http://myaccount.copyright.com)

Terms and Conditions

1. The materials you have requested permission to reproduce (the "Materials") are protected by copyright.

2. You are hereby granted a personal, non-exclusive, non-sublicensable, non-transferable, worldwide, limited license to reproduce the Materials for the purpose specified in the licensing process. This license is for a one-time use only with a maximum distribution equal to the number that you identified in the licensing process. Any form of republication granted by this licence must be completed within two years of the date of the grant of this licence (although copies prepared before may be distributed thereafter). The Materials shall not be used in any other manner or for any other purpose. Permission is granted subject to an appropriate acknowledgement given to the author, title of the material/book/journal and the publisher. You shall also duplicate the copyright notice that appears in the Wiley publication in your use of the Material. Permission is also granted on the understanding that nowhere in the text is a previously published source acknowledged for all or part of this Material. Any third party material is expressly excluded from this permission.

3. With respect to the Materials, all rights are reserved. Except as expressly granted by the terms of the license, no part of the Materials may be copied, modified, adapted (except for minor reformatting required by the new Publication), translated, reproduced, transferred or distributed, in any form or by any means, and no derivative works may be made based on the Materials without the prior permission of the respective copyright owner. You may not alter, remove or suppress in any manner any copyright, trademark or other notices displayed by the Materials. You may not license, rent, sell, loan, lease, pledge, offer as security, transfer or assign the Materials, or any of the rights granted to you hereunder to any other person.

4. The Materials and all of the intellectual property rights therein shall at all times remain the exclusive property of John Wiley & Sons Inc or one of its related companies (WILEY) or their respective licensors, and your interest therein is only that of having possession of and the right to reproduce the Materials pursuant to Section 2 herein during the continuance of this Agreement. You agree that you own no right, title or interest in or to the Materials or any of the intellectual property rights therein. You shall have no rights hereunder other than the license as provided for above in Section 2. No right, license or interest to any trademark, trade name, service mark or other branding ("Marks") of WILEY or its licensors is granted hereunder, and you agree that you shall not assert any such right, license or interest with respect thereto.

5. NEITHER WILEY NOR ITS LICENSORS MAKES ANY WARRANTY OR REPRESENTATION OF ANY KIND TO YOU OR ANY THIRD PARTY, EXPRESS, IMPLIED OR STATUTORY, WITH RESPECT TO THE MATERIALS OR THE ACCURACY OF ANY INFORMATION CONTAINED IN THE MATERIALS, INCLUDING, WITHOUT LIMITATION, ANY IMPLIED WARRANTY OF MERCHANTABILITY, ACCURACY, SATISFACTORY QUALITY, FITNESS FOR A PARTICULAR PURPOSE, USABILITY, INTEGRATION OR NON-INFRINGEMENT AND ALL SUCH WARRANTIES ARE HEREBY EXCLUDED BY WILEY AND ITS LICENSORS AND WAIVED BY YOU.

6. WILEY shall have the right to terminate this Agreement immediately upon breach of this Agreement by you.

7. You shall indemnify, defend and hold harmless WILEY, its Licensors and their respective directors, officers, agents and employees, from and against any actual or threatened claims, demands, causes of action or proceedings arising from any breach of this Agreement by you.

8. IN NO EVENT SHALL WILEY OR ITS LICENSORS BE LIABLE TO YOU OR ANY OTHER PARTY OR ANY OTHER PERSON OR ENTITY FOR ANY SPECIAL, CONSEQUENTIAL, INCIDENTAL, INDIRECT, EXEMPLARY OR PUNITIVE DAMAGES, HOWEVER CAUSED, ARISING OUT OF OR IN CONNECTION WITH THE DOWNLOADING, PROVISIONING, VIEWING OR USE OF THE MATERIALS REGARDLESS OF THE FORM OF ACTION, WHETHER FOR BREACH OF CONTRACT, BREACH OF WARRANTY, TORT, NEGLIGENCE, INFRINGEMENT OR OTHERWISE (INCLUDING, WITHOUT LIMITATION, DAMAGES BASED ON LOSS OF PROFITS, DATA, FILES, USE, BUSINESS OPPORTUNITY OR CLAIMS OF THIRD PARTIES), AND WHETHER OR NOT THE PARTY HAS BEEN ADVISED OF THE POSSIBILITY OF SUCH DAMAGES. THIS LIMITATION SHALL APPLY NOTWITHSTANDING ANY FAILURE OF ESSENTIAL PURPOSE OF ANY LIMITED REMEDY PROVIDED HEREIN.

9. Should any provision of this Agreement be held by a court of competent jurisdiction to be illegal, invalid, or unenforceable, that provision shall be deemed amended to achieve as nearly as possible the same economic effect as the original provision, and the legality, validity and

enforceability of the remaining provisions of this Agreement shall not be affected or impaired thereby.

10. The failure of either party to enforce any term or condition of this Agreement shall not constitute a waiver of either party's right to enforce each and every term and condition of this Agreement. No breach under this agreement shall be deemed waived or excused by either party unless such waiver or consent is in writing signed by the party granting such waiver or consent. The waiver by or consent of a party to a breach of any provision of this Agreement shall not operate or be construed as a waiver of or consent to any other or subsequent breach by such other party.

11. This Agreement may not be assigned (including by operation of law or otherwise) by you without WILEY's prior written consent.

12. Any fee required for this permission shall be non-refundable after thirty (30) days from receipt.

13. These terms and conditions together with CCC's Billing and Payment terms and conditions (which are incorporated herein) form the entire agreement between you and WILEY concerning this licensing transaction and (in the absence of fraud) supersedes all prior agreements and representations of the parties, oral or written. This Agreement may not be amended except in writing signed by both parties. This Agreement shall be binding upon and inure to the benefit of the parties' successors, legal representatives, and authorized assigns.

14. In the event of any conflict between your obligations established by these terms and conditions and those established by CCC's Billing and Payment terms and conditions, these terms and conditions shall prevail.

15. WILEY expressly reserves all rights not specifically granted in the combination of (i) the license details provided by you and accepted in the course of this licensing transaction, (ii) these terms and conditions and (iii) CCC's Billing and Payment terms and conditions.

16. This Agreement will be void if the Type of Use, Format, Circulation, or Requestor Type was misrepresented during the licensing process.

17. This Agreement shall be governed by and construed in accordance with the laws of the State of New York, USA, without regards to such state's conflict of law rules. Any legal action, suit or proceeding arising out of or relating to these Terms and Conditions or the breach thereof shall be instituted in a court of competent jurisdiction in New York County in the State of New York in the United States of America and each party hereby consents and submits to the personal jurisdiction of such court, waives any objection to venue in such court and consents to service of process by registered or certified mail, return receipt requested, at the last known address of such party.

Wiley Open Access Terms and Conditions

All research articles published in Wiley Open Access journals are fully open access: immediately freely available to read, download and share. Articles are published under the terms of the Creative Commons Attribution Non Commercial License. which permits use, distribution and reproduction in any medium, provided the original work is properly cited and is not used for commercial purposes. The license is subject to the Wiley Open Access terms and conditions: Wiley Open Access articles are protected by copyright and are posted to repositories and websites in accordance with the terms of the Creative Commons Attribution Non Commercial License. At the time of deposit, Wiley Open Access articles include all changes made during peer review, copyediting, and publishing. Repositories and websites that host the article are responsible for incorporating any publisher-supplied amendments or retractions issued subsequently. Wiley Open Access articles are also available without charge on Wiley's publishing platform, **Wiley Online Library** or any successor sites.

Use by non-commercial users

For non-commercial and non-promotional purposes individual users may access, download, copy,

display and redistribute to colleagues Wiley Open Access articles, as well as adapt, translate, text- and data-mine the content subject to the following conditions:

- The authors' moral rights are not compromised. These rights include the right of "paternity" (also known as "attribution" - the right for the author to be identified as such) and "integrity" (the right for the author not to have the work altered in such a way that the author's reputation or integrity may be impugned).
- Where content in the article is identified as belonging to a third party, it is the obligation of the user to ensure that any reuse complies with the copyright policies of the owner of that content.
- If article content is copied, downloaded or otherwise reused for non-commercial research and education purposes, a link to the appropriate bibliographic citation (authors, journal, article title, volume, issue, page numbers, DOI and the link to the definitive published version on Wiley Online Library) should be maintained. Copyright notices and disclaimers must not be deleted.
- Any translations, for which a prior translation agreement with Wiley has not been agreed, must prominently display the statement: "This is an unofficial translation of an article that appeared in a Wiley publication. The publisher has not endorsed this translation."

Use by commercial "for-profit" organisations

Use of Wiley Open Access articles for commercial, promotional, or marketing purposes requires further explicit permission from Wiley and will be subject to a fee. Commercial purposes include:

- Copying or downloading of articles, or linking to such articles for further redistribution, sale or licensing;
- Copying, downloading or posting by a site or service that incorporates advertising with such content;
- The inclusion or incorporation of article content in other works or services (other than normal quotations with an appropriate citation) that is then available for sale or licensing, for a fee (for example, a compilation produced for marketing purposes, inclusion in a sales pack)
- Use of article content (other than normal quotations with appropriate citation) by for-profit organisations for promotional purposes
- Linking to article content in e-mails redistributed for promotional, marketing or educational purposes;
- Use for the purposes of monetary reward by means of sale, resale, licence, loan, transfer or other form of commercial exploitation such as marketing products
- Print reprints of Wiley Open Access articles can be purchased from: corporatesales@wiley.com

Other Terms and Conditions:

BY CLICKING ON THE "I AGREE..." BOX, YOU ACKNOWLEDGE THAT YOU HAVE READ AND FULLY UNDERSTAND EACH OF THE SECTIONS OF AND PROVISIONS SET FORTH IN THIS AGREEMENT AND THAT YOU ARE IN AGREEMENT WITH AND ARE WILLING TO ACCEPT ALL OF YOUR OBLIGATIONS AS SET FORTH IN THIS AGREEMENT.

v1.7

Gratis licenses (referencing $0 in the Total field) are free. Please retain this printable

license for your reference. No payment is required.

If you would like to pay for this license now, please remit this license along with your payment made payable to "COPYRIGHT CLEARANCE CENTER" otherwise you will be invoiced within 48 hours of the license date. Payment should be in the form of a check or money order referencing your account number and this invoice number RLNK11036956.
Once you receive your invoice for this order, you may pay your invoice by credit card. Please follow instructions provided at that time.

Make Payment To:
Copyright Clearance Center
Dept 001
P.O. Box 843006
Boston, MA 02284-3006

For suggestions or comments regarding this order, contact Rightslink Customer Support: customercare@copyright.com or +1-877-622-5543 (toll free in the US) or +1-978-646-2777.